Prediction of Performance and Maneuvering Dynamics for Marine Vehicles Applied to DDG-1000

by

Louis-Philippe M. Menard

Submitted to the Department of Mechanical Engineering
In partial fulfillment of the requirements for the degree of

Master of Science in Naval Architecture and Marine Engineering
and
Master of Science in Mechanical Engineering

at the

MASSACHUSETTS INSTITUTE OF TECHNOLOGY

June 2010

Author.....
Department of Mechanical Engineering
June 4, 2010

Certified by.....
Michael S. Triantafyllou
Professor, Mechanical Engineering
Thesis Supervisor

Accepted by.....
David E. Hardt
Ralph E. and Eloise F. Cross Professor of Mechanical Engineering
Chairman, Department Committee on Graduate Students

This page intentionally blank

Prediction of Performance and Maneuvering Dynamics for Marine Vehicles Applied to DDG-1000

by

Louis-Philippe M. Menard

Submitted to the Department of Mechanical Engineering
In partial fulfillment of the requirements for the degree of

Master of Science in Naval Architecture and Marine Engineering
and
Master of Science in Mechanical Engineering

Abstract

Being able to accurately model the performance of ships is an integral part of the ship design process. A considerable amount of money is invested into predicting how a ship will maneuver in a given sea state. Furthermore, it is vital to understand the powering requirements and potential limitations of the ship design. Typically, a physical scale model of the ship is constructed and experimented on in a tow tank to determine the hydrodynamic characteristics of the ship to be built. This can also be expensive. Therefore, there is considerable interest in developing a means to predict the hydrodynamic performance of a ship using alternative means. This thesis presents an analytical determination of the hydrodynamic coefficients for the DDG-1000 and compares them to an existing physical model with the intent to use the physical model as a substitute.

Using analytical methods from several established sources, this thesis develops a simulated model for the DDG-1000 that is consistent with expected performance of a ship of this size and class. In addition, this thesis presents a model for the all-electric ship using azimuthing propellers. The analytically determined maneuvering dynamics are applied to the full all-electric ship system model, which incorporates the main generating engines through the power electronics to the motor and propulsion shafts. The results of the simulation form a baseline, from which future optimization of the model can occur.

Thesis Supervisor: Michael S. Triantafyllou
Title: Professor of Mechanical Engineering

This page intentionally blank

Acknowledgements

I would first like to thank my advisor, Professor Triantafyllou for his continued support, suggestions and encouragement. In addition, I would like to acknowledge Professor Chryssostomidis and the Sea Grant Foundation for providing me the opportunity to contribute to my understanding of ship maneuvering dynamics as well as to the USN's interests. Next, it is important I thank my colleagues Kyle Schmitt and Ilkay Erselcan without whose mutual guidance we would not have accomplished so much.

Lastly, and more importantly, it is necessary I thank my family and Teddy for their undying love and support and ensuring I maintained stalwart dedication until the end. And, of course, I wish to thank Rhonda for absolutely everything.

L.P.M. Menard
Cambridge, Massachusetts

This page intentionally blank

Contents

List of Figures

List of Tables

This page intentionally blank

Chapter 1

Introduction

1.1 Motivation

The all-electric ship is the next stage of technological development for the surface warship. Conventional surface ship design has strongly delineated boundaries representing the divide between propulsion and auxiliary systems and combat-related systems. Submarines, on the other hand, readily incorporate the two seemingly disparate system groups into a fully integrated all-electric weapons platform. Submarines have been doing this for many decades. Indeed, the transition from conventional propulsion (for example, diesel and gas turbine engines driving a reduction gearbox) to integrated electric propulsion presents a marked shift in how future surface combatants will engage in a hostile threat environment. The advent of cutting edge energy weapons and the need to ensure continuous tracking of potential threats requires a significant demand on the existing ship's electrical loading. Add to this the ship's propulsion requirements which, in a threat environment, is typically at the higher end of the speed spectrum, and it poses a challenge to future ship designers and builders who must forge new territory, often making bold assumptions in the process.

The United States Navy (USN) is building the all-electric ship class DDG-1000 to meet the goals above. As such, it is useful to create models that can predict the maneuvering

and propulsive performance of the full-scale ship. This thesis presents a maneuvering model of the DDG-1000 within the framework of the all-electric ship propulsion system such that ship performance assumptions can be predicted, validated and optimized without a physical model of the actual DDG-1000. In addition, some optimization analysis is performed to permit selection of a propulsion system that will minimize output torque and maximize thrust while remaining within the propeller cavitation-free operating zone.

1.2 Background

There has been extensive work in the development of maneuvering models for numerous classes of ships. Previous model-based research has focused on the hydrodynamics, drag, and efficiency of azimuthing propulsion units with emphasis on the unsteady forces and dynamics (Stettler, [18]) in an attempt to apply the model to the full-scale ship. Next, this model was applied to linear control technologies in order to apply control the nonlinear dynamics of ships using podded propulsion (Greytak, [5]).

Currently, and beginning in early 2009, research has progressed on creating a propulsion system model of an all-electric ship based on the USN ship class, DDG-1000. The propulsion system model explores the dynamics and interactions between the GE LM2500 gas turbines through the electrical generators and associated power electronics and to the propulsors as seen in system architecture diagram in Figure 1.1. With the inclusion of the maneuvering dynamics (including rudder interaction) and nonlinear wave forcing, the system behaviour can be analyzed and predicted. In addition, there is considerable interest in the application of azimuthing pods to the all-electric ship model described.

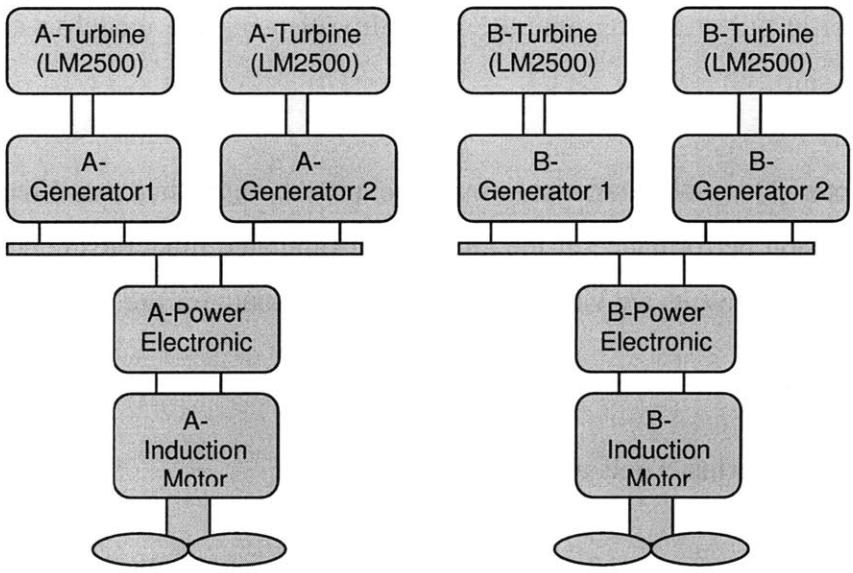

Figure 1.1: Example propulsion system architecture for all-electric ship.

This thesis builds upon the extensive research completed in support of the Sea Grant program and purports to use the physical model of the kayak analyzed for Stettler [18] and Greytak [5]. In order to use this model, however, this thesis demonstrates through analytical methods that the hydrodynamic coefficients measured for the kayak can be used as a reasonable approximation to the full-scale DDG-1000.

1.3 Thesis Preview

This thesis documents an overall effort to apply the nonlinear maneuvering dynamics to the all-electric ship problem through extensive detailed numerical simulation. In time, the simulation results will be validated against the performance of the full-scale vessel. For now, though, the simulation results are validated against other predictive methods and tools to estimate what is a reasonable performance objective for the ship.

Chapter 2 presents an overview of the derivation of the nonlinear maneuvering dynamics for conventional and azimuth podded propulsors as it pertains to the DDG-1000. The non-linear dynamics are derived using analytical methods and compared to a physical

model in order to determine the feasibility of using the model to approximate the full-scale ship.

Chapter 3 explores simulations of the model to predict the directional stability and propulsion performance of the DDG-1000 simulated model using conventional propeller shafts. The results are validated against existing data for the full-scale ship.

1.4 Software Tools and Simulated Model

All computational work for this project was performed using Mathworks' MATLAB and Simulink software, with the Control Systems Toolbox receiving the heaviest use. Data characterizing the hull was provided in [Stettler, 18] and used to create a nonlinear model and simulation of the system.

Chapter 2

Dynamics of Ship Motion

This chapter provides a framework from which the maneuvering dynamics of the simulated model of the DDG-1000 is generated by determining the non-linear hydrodynamic coefficients related to the full-scale ship and making a comparison against those of the model kayak. By doing so, this validates the kayak as a usable model for the all-electric ship. Of course, the full model applies simulations of the engine propulsion control modules and power electronics distribution (as shown in Figure 2.1); however, the scope of this thesis is on the maneuvering dynamics only.

The chapter sections are organized as follows:

2.1 A model for a marine vehicle maneuvering in the horizontal plane. The overall model for the all-electric ship propulsion and maneuvering interaction is introduced and discussed.

2.2 Non-linear governing equations of motion. A derivation of the non-linear governing equations of motion is presented using an expanded Taylor series form for the hydrodynamic coefficients.

2.3 Derivation of non-linear hydrodynamic coefficients. Various methods are employed to determine the value of the coefficients identified in the preceding section. Methods include slender-body and foil theory, and parametric analysis of model tests. The results are compared against PMM data taken of the physical scale model.

2.4 The modeled forces are modified to account for a ship using azimuthing podded propulsion.

In the final section, the derived models are compared against each other and validated against the PMM data.

2.1 A Model for a Marine Vehicle Maneuvering in the Horizontal Plane

Developing a comprehensive maneuvering model for the all-electric ship involves incorporating simulated components from the main driving engines to the propellers and changing the inputs to these components as the vessel maneuvers through the horizontal plane. Figure 2.1 shows an example model for an all-electric ship. The interrelationship between the torque generated at the driving engine and the ship's speed can be clearly seen. Therefore, it is important that a useful model of the maneuvering dynamics is generated to best predict these interactions.

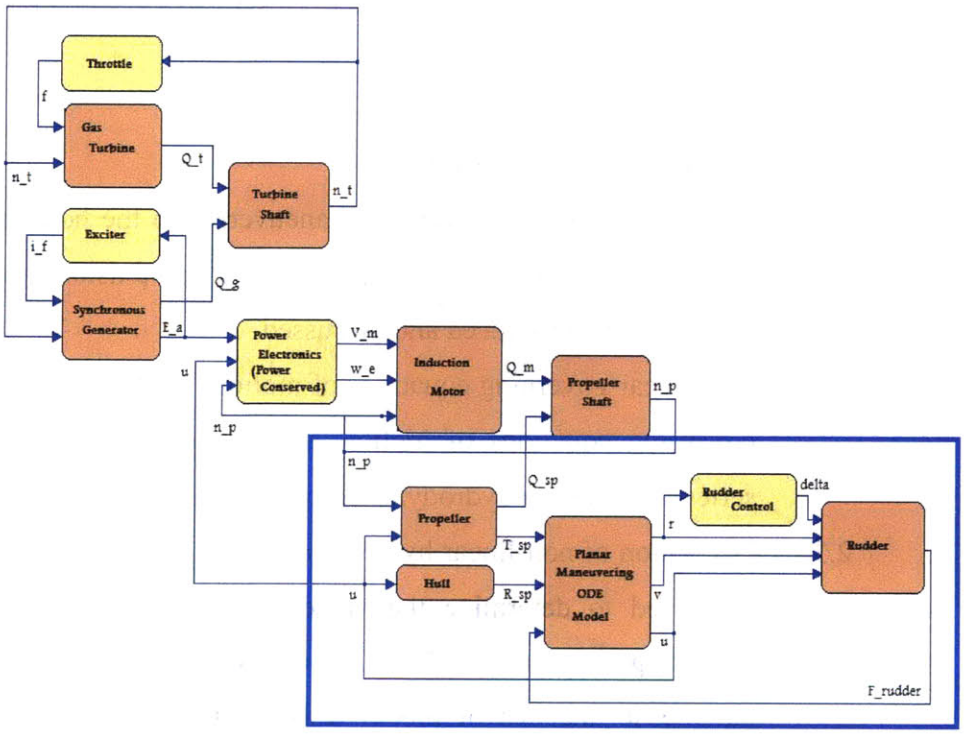

Figure 2.1: Example model configuration diagram that includes maneuvering dynamics (boxed).

Indeed, correctly modeling the maneuvering dynamics is important should one want to apply maneuvering and heading control as in Figure 2.2.

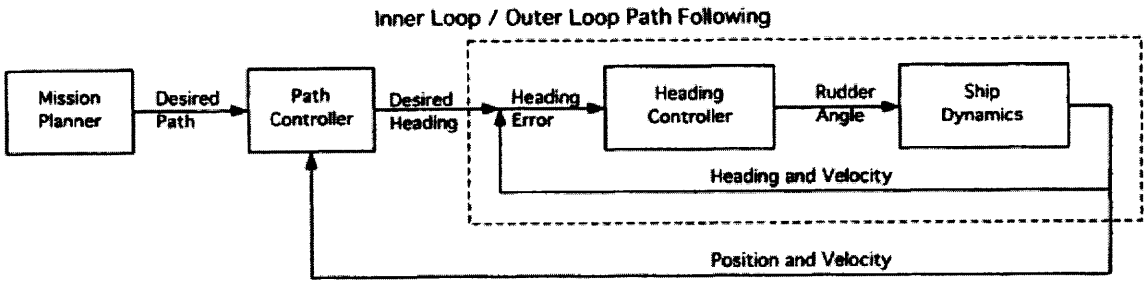

Figure 2.2: A typical controller system where the path controller generates a desired heading and the heading controller generates a desired rudder angle.

Validity of Model and Vessel Speed Range

Because the kayak is not a physical model of the DDG-1000, it is important that the simulations are performed within a valid speed range, one that is useful for analysis (i.e. the design speed of the ship). It is noted that, though the physical model upon which the research in [18] is based, was originally applied to the azimuthing podded propulsion problem, the same model can be applied to a conventional propulsion design over a range of operating speeds using Froude similitude [22]. The condition for this is for the model's Reynold's number to be above critical. For the nominal kayak speed of 1.6 m/s:

$$\text{Reynold's Number:} \quad \mathrm{Re}_m = \frac{U_m L_m}{\upsilon} \approx 6\times10^5 \geq \mathrm{Re}_{crit}$$

Next, using the nominal kayak speed, the full-scale vessel speed that permits Froude similitude can be determined:

$$\text{Froude Similitude:} \quad Fr = \frac{U}{\sqrt{gL}} \Rightarrow Fr_{model} = 0.2672$$

Therefore, for $Fr_{model} = Fr_{vessel}$ the Simulink model should be analyzed about:

$$U_{vessel} = 11.31 \text{ m/s} = 22 \text{ knots}$$

2.2 Non-Linear Governing Equations of Motion

Begin by considering the rigid body dynamics of the vessel of interest with a coordinate system affixed on the body, as shown in Figure 2.3. This convention gives the following orientation:

x, u, ψ, p is forward distance, surge velocity, and roll angle

y, v, θ, q is port motion, sway velocity, and pitch angle

z, w, φ, r is vertical motion, heave velocity, and yaw angle

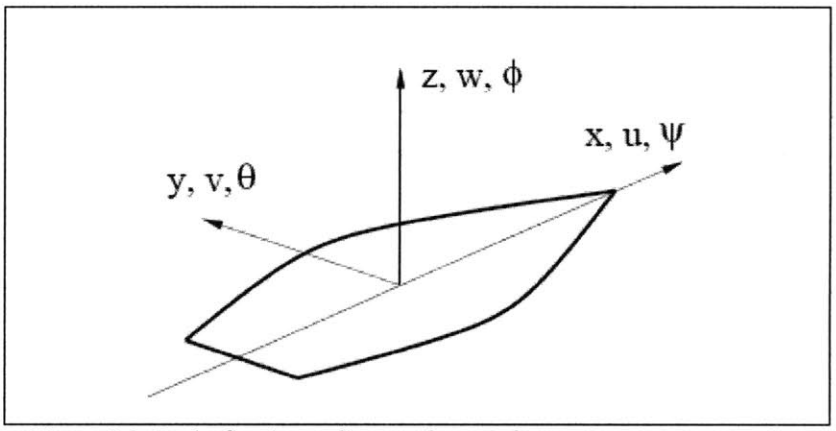

Figure 2.3: Body-fixed coordinate reference frame.

Consider first linear momentum. From ([1], [21]), begin with a fixed body on a rotating system to give the complete vector equation of the linear momentum of the body in Equation 2.1:

$$\vec{F} = \sum_{i=1}^{N} \vec{Fi} = m\left(\frac{\partial \vec{u_o}}{\partial t} + \vec{\omega} \times \vec{u_o} + \frac{d\vec{\omega}}{dt} \times \vec{r_G} + \vec{\omega} \times (\vec{\omega} \times \vec{r_G})\right) \qquad (2.1)$$

where

$\vec{u_o}$ = {u, v, w} is the body-referenced velocity;

$\vec{r_G}$ = {x_G, y_G, z_G} is the body-referenced location of center of mass;

$\vec{\omega}$ = {p, q, r} is the rotation vector in body coordinates;

$\vec{F}$ = {X, Y, Z} is the external force in body coordinates.

Expanding (2.1), the resulting linear momentum equations are:

$$X = m[\frac{\partial u}{\partial t} + qw - rv + \frac{dq}{dt} z_G - \frac{dr}{dt} y_G + (qy_G + rz_G)p - (q^2 + r^2)x_G]$$

$$Y = m[\frac{\partial v}{\partial t} + ru - pw + \frac{dr}{dt} x_G - \frac{dp}{dt} z_G + (rz_G + px_G)q - (r^2 + p^2)y_G] \quad (2.2)$$

$$Z = m[\frac{\partial w}{\partial t} + pv - qu + \frac{dp}{dt} y_G - \frac{dq}{dt} x_G + (px_G + qy_G)r - (p^2 + q^2)z_G]$$

Considering port and starboard symmetries about the x-z plane, the origin can be placed on the centerline of the vessel, making y_G=0. Next, consider only vessel motions in the horizontal plane only and the vertical center of gravity can be conveniently placed anywhere, thus choose the point such that z_G=0. Similarly, ignore heave (w=0), roll (p=0), pitch (q=0) and Z-forces entirely. Applying these simplifications to Equation (2.2) yields:

$$X = m[\frac{\partial u}{\partial t} - rv - r^2 x_G]$$

$$Y = m[\frac{\partial v}{\partial t} + ru + \dot{r}x_G] \quad (2.3)$$

Now consider angular momentum following the same steps from the linear momentum derivation to arrive at Equation 2.4:

$$\vec{M} = \sum_{i=1}^{N} (\vec{Mi} + \vec{r_i} \times \vec{F_i}) = \sum_{i=1}^{N} m_i \vec{r_i} \times [\frac{\partial \vec{u_o}}{\partial t} + \vec{\omega} \times \vec{u_o}] + \sum_{i=1}^{N} m_i \vec{r_i} \times (\frac{\partial \vec{\omega}}{\partial t} \times \vec{r_i}) + \sum_{i=1}^{N} m_i \vec{r_i} \times (\vec{\omega} \times (\vec{\omega} \times \vec{r_i})) \quad (2.4)$$

where $\vec{M}$ = {K, M, N} is the total moment acting on the body.

Expanding (2.4) and considering only angular motion in the horizontal plane, the non-linear equation for yaw moment is given below.

$$N = I_{zx}\dot{p} + I_{zy}\dot{q} + I_{zz}\dot{r} + (I_{yy} - I_{xx})pq + I_{xy}(p^2 - q^2) + I_{yz}pr \\ -I_{xz}qr + m[x_G(\dot{v} + ru - pw) - y_G(\dot{u} + qw - rv)] \tag{2.5}$$

Next, impose the same assumptions as in the linear momentum case:

$$y_G = z_G = w = p = q = 0;$$

This gives the following equation for yaw moment, N:

$$N = I_{zz}\dot{r} + mx_G(\dot{v} + ru) \tag{2.6}$$

The resulting complete non-linear equations of motion in the horizontal plane are summarized below:

COMPLETE NON-LINEAR EQUATIONS OF MOTION IN THE HORIZONTAL PLANE

$$X = m[\frac{\partial u}{\partial t} - rv - r^2 x_G]$$

$$Y = m[\frac{\partial v}{\partial t} + ru + \dot{r}x_G] \tag{2.7}$$

$$N = I_{zz}\dot{r} + mx_G(\dot{v} + ru)$$

X, Y, and N are the external body forces and moments (due to hydrodynamics, actuators, etc.) applied in the body-referenced directions of x, y, and z, respectively.

2.2.1 Expansion of External Forces

Up to this point, the sum of all hydrodynamic forces have been represented as X, Y, and N. By applying a 3rd order Taylor series expansion, the forces are expanded to make a representation of each contributing component of the respective hydrodynamic forces (i.e. X = X(u,v,r), Y = Y(u,v,r) and N = N(u,v,r). The 3rd order expansion has been found to provide a useful measure of accuracy over a wide range ([1], [21]) . Following the Taylor expansion, the following facts and assumptions (from [23]) simplify the terms:

- Retain only 1st order acceleration terms. Based on Newton's second law, we expect the inertia terms from the fluid to be linearly dependent on acceleration.

- Do not include terms coupling velocities and accelerations, because based on Newton's Second Law we expect inertia forces to depend on acceleration alone.

- Exploit the port / starboard symmetry of the ship, in order to eliminate a certain number of coefficients which are either zero or very small:
  In terms of the fluid force X, the port / starboard symmetry can be decoded as:
  - X(u, v, r=0)=X(u, -v, r=0) (X is a symmetric function of v when r=0)
  - X(u, v=0, r)=X(u, v=0, -r) (X is a symmetric function of r when v=0)

  The above relations imply that all odd derivatives of X with respect to v at v=0 are zero, when r=0, and similarly for r. In summary, symmetry provides the following zero coefficients:

$$X_v = 0, \quad X_{vvv} = 0, \quad X_{vu} = 0, \quad X_{vuu} = 0$$
$$X_r = 0, \quad X_{rrr} = 0, \quad X_{ru} = 0, \quad X_{ruu} = 0,$$

In terms of the fluid force Y, the port / starboard symmetry implies that this force must be an anti-symmetric function of v when r=0, and likewise for r:

- Y(u, v, r=0)=-Y(u, -v, r=0) (Y is an anti-symmetric function of v when r=0)
- Y(u, v=0, r)=-Y(u, v=0, -r) (Y is an anti-symmetric function of r when v=0)

The above relations imply that all even derivatives of Y with respect to v at v=0 are zero, when r=0, and similarly for r. In summary, symmetry provides the following zero coefficients:

$$Y_{vv} = 0, \qquad Y_{vvu} = 0$$
$$Y_{rr} = 0, \qquad Y_{rru} = 0$$

The derivation of the fluid moment N follows the same exact steps as for the side force Y, i.e. the same symmetries apply. As a result, the following coefficients are zero:

$$N_{vv} = 0, \qquad N_{vvu} = 0$$
$$N_{rr} = 0, \qquad N_{rru} = 0$$

- In general, a propeller introduces an asymmetry port / starboard since it rotates in a certain direction. In the case of DDG-1000, the full-scale vessel is equipped with two fixed-pitch propellers rotating opposite of each other, which counters this asymmetry:

$$Y_u = 0 \qquad Y_{uu} = 0$$
$$N_u = 0 \qquad N_{uu} = 0$$

- Steady-state effects consist of forces and moments that are present during steady-state motion. At steady-state, the ship resistance is represented by X_0 when all other dynamic terms are zero. Y_0 and N_0 represent steady-state sway and yaw moment, respectively. These forces and moments are present primarily on single-screw ships and represent the tendency of the ship to translate or rotate in a particular direction when propeller thrust is small.

DDG 1000 has twin screws rotating in opposite directions, therefore, the following steady-state forces and moments are zero:

$$Y_0 = 0$$

$$N_0 = 0$$

Steady-state hull resistance, X_0, can be derived as follows:

$$R_s = \frac{1}{2}\rho C_R A_w U^2 /(1-t) \tag{2.8}$$

where C_R is the resistant coefficient based on Reynold's number and is a combination of frictional and form drag, and A_w is the total wetted surface area. The term $(1-t)$ represents the thrust deduction factor, which accounts for the additional drag induced by the propellers.

Applying the above simplifications the expanded hydrodynamic expressions of X, Y, N results in Equation 2.9:

$$\begin{aligned}
&m(\dot{u} - rv - r^2 x_G) = X_o + X_{\dot{u}}\dot{u} + X_u u + X_{uu}u^2 + X_{uuu}u^3 + X_{vv}v^2 + X_{rr}r^2 + X_{vvu}v^2 u + \\
&+ X_{rru}r^2 u + X_{vr}vr + X_{vru}vru + Ext.Forces \\
&m(\dot{v} + ru + \dot{r}x_G) = Y_{\dot{v}}\dot{v} + Y_{\dot{r}}\dot{r} + Y_v v + Y_{vvv}v^3 + Y_r r + Y_{rrr}r^3 + Y_{vrr}vr^2 + Y_{vu}vu + Y_{ru}ru \\
&+ Y_{vuu}vu^2 + Y_{rvv}rv^2 + Y_{ruu}ru^2 + Ext.Forces + ActuatorTerms \\
&I_{zz}\dot{r} + mx_G(\dot{v} + ru) = N_{\dot{v}}\dot{v} + N_{\dot{r}}\dot{r} + N_v v + N_{vvv}v^3 + N_r r + N_{rrr}r^3 + N_{vrr}vr^2 \\
&+ N_{vu}vu + N_{ru}ru + N_{vuu}vu^2 + N_{rvv}rv^2 + N_{ruu}ru^2 + ExtMoments + ActuatorTerms
\end{aligned} \tag{2.9}$$

The equations (2.9) describe how the ship will respond to external forces and moments acting in the three degrees of freedom. External forces and moments include those generated by propulsors and surface actuators (rudders, fins), in addition to the influencing terms that these surfaces create.

2.3 Derivation of Non-Linear Hydrodynamic Coefficients

The prediction of hull hydrodynamic maneuvering forces is discussed in many references ([1],[3],[4],[6],[9],[10],[13],[14],[16],[17],[18],[20],[21]). This section provides an overview of several methods and presents a detailed summary comparison between these methods and the 'exact' value of the coefficients as determined by the PMM. The PMM determines the exact values of the hydrodynamic coefficients for movements in the horizontal plane. By using parametric and analytical methods, the non-linear hydrodynamic coefficients can be predicted and compared against the measured values.

2.3.1 Linear Hydrodynamic Coefficients

The linear hydrodynamic coefficients can be predicted using the equations developed by Inoue at al. [10], and also derived in [14], who estimated hull maneuvering forces based on physical considerations and model data. The linear non-dimensional terms are given by Equations 2.10. Inoue et al. non-dimensionalized using ship length and ship draft as the distance parameter. For the purposes of this thesis, the terms are non-dimensionalized with respect to ship length only by applying a correction factor of (T_{mid}/L).

$$
\begin{aligned}
Y'_v &= -\left(\frac{\pi}{2}\frac{T_{mid}}{L}\right)\left(1+\frac{2t_{stern}}{3T_{mid}}\right)\left(\frac{T_{mid}}{L}\right) \\
Y'_r &= \frac{\pi}{2}\frac{T_{mid}}{L}\left(1+0.8\frac{t_{stern}}{T_{mid}}\right)\left(\frac{T_{mid}}{L}\right) \\
N'_v &= -\frac{2T_{mid}}{L}\left(1-\frac{0.27}{l_\alpha}\frac{t_{stern}}{T_{mid}}\right)\left(\frac{T_{mid}}{L}\right) \\
N'_r &= -\left[0.54\frac{2T_{mid}}{L}-\left(\frac{2T_{mid}}{L}\right)^2\right]\left(1+0.30\frac{t_{stern}}{T_{mid}}\right)\left(\frac{T_{mid}}{L}\right)
\end{aligned}
\qquad (2.10)
$$

where T_{mid} is the draft at midships, C_B is the block coefficient, and t_{stern} is the trim at the stern (equal to zero).

The term l_α is given by:

$$l_\alpha = \frac{2T_{mid}}{\pi T_{mid} + 1.4C_B B} \tag{2.11}$$

2.3.2 Non-Linear Hydrodynamic Coefficients

The principal components of hydrodynamic damping are skin friction, due to boundary layers, which may be partly laminar and partly turbulent, and damping due to separation and vortex shedding. The ship's Reynold's number permits understanding of which regime that the vessel is operating in as it represents the ratio of inertial to viscous forces:

$$\mathrm{Re} = \frac{Ul}{\upsilon} \tag{2.12}$$

The ship operates at a Reynold's number of 1.23e6, which is in the turbulent regime. This will help determine the drag coefficient of the ship.

Using known analytical methods, the non-linear hydrodynamic coefficients can be calculated up to second-order. Third-order terms are not within the scope of calculations for this thesis.

2.3.2.1 Axial Drag

The ship's axial drag can be expressed using the following empirical relationship, noted earlier as Equation (2.13):

$$R_s = \frac{1}{2}\rho C_R A_w u|u| \tag{2.13}$$

This equation yields the following non-linear axial drag coefficient:

$$X_{u|u|} = -\frac{1}{2}\rho C_R A_w \tag{2.14}$$

where C_R is the resistance coefficient based on Reynold's number and is a combination of frictional and form drag, and A_w is the total wetted surface area. The term $(1-t)$ represents the thrust deduction factor, which accounts for the additional drag induced by the propellers.

The resistance coefficient is approximated and derived from the 1957 ITTC line [23] as:

$$C_R = \frac{0.075}{(\log_{10}\mathrm{Re}-2)^2} \approx 0.0048 \tag{2.15}$$

2.3.2.2 Crossflow Drag

The non-linear non-dimensional terms developed by Inoue et al. [10] are given as Equations 2.16.

$$\begin{aligned}
Y'_{v|v|} &= \left(0.09-6.5(1-C_B)\frac{T_{mid}}{B}\right)\left(\frac{T_{mid}}{L}\right) \\
Y'_{v|r|} &= \left(-0.44+1.78(1-C_B)\frac{T_{mid}}{B}\right)\left(\frac{T_{mid}}{L}\right) \\
Y'_{r|r|} &= 0.0 \\
N'_{vr^2} &= 0.0 \\
N'_{r|r|} &= \begin{cases} -0.060 & \frac{C_B B}{L} < 0.06 \\ -0.146+1.8\frac{C_B B}{L}-6\left(\frac{C_B B}{L}\right)^2 & 0.06 \le \frac{C_B B}{L} \le 0.2 \\ -0.026 & \frac{C_B B}{L} > 0.2 \end{cases} \\
N'_{rv^2} &= -0.2
\end{aligned} \tag{2.16}$$

The terms $Y_{r|r|}$ and N_{vr^2} are set to zero because of the significant scatter in measured values. This approach for predicting hull maneuvering coefficients is intended for ships with a tendency to have rectangular lateral profiles and may not be the most appropriate for application to naval warships. Indeed, the definition of the hydrodynamic coefficients set forth in Section 2.2.1 set many of these terms to zero based on hull symmetry.

2.3.2.3 Added Mass

A vessel's added mass is a measure of the mass of moving water when the body accelerates and are expressed by the following inertial matrix. Only the terms in the horizontal plane are examined and, with port-starboard symmetry, the matrix reduces to:

$$M_a = \begin{bmatrix} X_{\dot{u}} & 0 & 0 \\ 0 & Y_{\dot{v}} & Y_{\dot{r}} \\ 0 & N_{\dot{v}} & N_{\dot{r}} \end{bmatrix} = \begin{bmatrix} -m_{11} & 0 & 0 \\ 0 & -m_{22} & -m_{26} \\ 0 & -m_{62} & -m_{66} \end{bmatrix} \tag{2.17}$$

Owing to bow-stern asymmetry, $m_{26} \neq m_{62}$.

Axial Added Mass

To predict the axial added mass, $X_{\dot{u}}$, the ship's hull form can be approximated by an ellipsoid for which the major axis is half the vessel's streamlined body length, L, and the minor axis is half the beam, B. From Blevins [2] and ([17], [21]), the axial added mass of an ellipsoid is given analytically as:

$$X_{\dot{u}} = -m_{11} = -\alpha \frac{4}{3} \rho \pi \left(\frac{L}{2}\right)\left(\frac{B}{2}\right)^2 \tag{2.18}$$

where α is an empirical parameter measured by Blevins and determined by the ratio of the vessel length to beam as shown in the table:

Table 2.1: Axial added mass parameter α [2].

L/B	α
2.0	0.2100
2.5	0.1563
3.0	0.1220
5.0	0.05912
7.0	0.03585
10.0	0.02071

Crossflow Added Mass

The ship's added mass is calculated using strip theory by approximating the hull form as a square plate of length equal to the draft at that longitudinal point along the hull. From [22], the added mass per unit length of a single square slice is given as:

$$m_a(x) = 4.754\,\rho a(x)^2 \tag{2.19}$$

where a(x) is half the length of the square's side as a function of the axial position along the hull; i.e. half of the draft at that point. Integrating Equation 2.19 over the length of the ship, the following expressions are derived for the cross-flow added-mass:

$$\begin{aligned} Y_{\dot{v}} &= -m_{22} = -\int_{stern}^{bow} m_a(x)dx \\ N_{\dot{v}} &= Y_{\dot{r}} = -m_{26} = -m_{62} = -\int_{stern}^{bow} x m_a(x)dx \\ N_{\dot{r}} &= -m_{66} = -\int_{stern}^{bow} x^2 m_a(x)dx \end{aligned} \tag{2.20}$$

Added Mass Cross-Terms

For the purposes of approximating the added mass cross-terms, it is convenient to assume that the added mass matrix given in (2.17) is symmetric; i.e. $\mathbf{M}_a = \mathbf{M}_a^T$. Now, the kinetic energy of the fluid, E_k, applied to the horizontal plane only, can be expressed as:

$$E_k = -\frac{1}{2}\underline{q}^T M_a \underline{q} = -\frac{1}{2}(X_{\dot{u}}u^2 + 2Y_{\dot{u}}vu + Y_{\dot{v}}v^2 + 2Y_{\dot{r}}vr + 2N_{\dot{u}}ur + N_{\dot{r}}r)^2 \tag{2.21}$$

where $\underline{q}^T = (u,v,r)$

To derive the inertia terms in the equations of motion from the kinetic energy, Kirchoff's relations are applied [21], which states that if $\vec{v}$ denotes the velocity vector and $\vec{w}$ the angular velocity, then the inertia terms, expressed in body-fixed coordinate system, are given by the expressions:

$$\begin{aligned} \vec{F} &= -\frac{\partial}{\partial t}\left(\frac{\partial E_k}{\partial \vec{v}}\right) - \vec{\omega} \times \left(\frac{\partial E_k}{\partial \vec{v}}\right) \\ \vec{Q} &= -\frac{\partial}{\partial t}\left(\frac{\partial E_k}{\partial \vec{\omega}}\right) - \vec{\omega} \times \left(\frac{\partial E_k}{\partial \vec{\omega}}\right) - \vec{v} \times \left(\frac{\partial E_k}{\partial \vec{v}}\right) \end{aligned} \tag{2.22}$$

Next, by applying Kirchoff's relations to the expression for kinetic energy with a symmetric added mass matrix, the following terms containing the fluid inertia forces are derived (noting that $X_{\dot{r}} = X_{\dot{v}} = Y_{\dot{u}} = N_{\dot{u}} = 0$):

$$\begin{aligned} X &= X_{\dot{u}}\dot{u} + -Y_{\dot{v}}vr - Y_{\dot{r}}r^2 \\ Y &= Y_{\dot{v}}\dot{v} + Y_{\dot{r}}\dot{r} + X_{\dot{u}}ur \\ N &= Y_{\dot{r}}\dot{v} + N_{\dot{r}}\dot{r} + Y_{\dot{r}}ur - (X_{\dot{u}} - Y_{\dot{v}})uv \end{aligned} \tag{2.23}$$

Therefore, the added mass cross-terms can be approximated as follows:

$$\begin{aligned} X_{vr} &= -Y_{\dot{v}} \\ X_{rr} &= -Y_{\dot{r}} \\ Y_{ru} &= X_{\dot{u}} \\ N_{ru} &= Y_{\dot{r}} \\ N_{vu\alpha} &= -(X_{\dot{u}} - Y_{\dot{v}}) \end{aligned} \tag{2.24}$$

The added mass cross-term $N_{vu\alpha}$ is known as the Munk moment [21] which relates the pure moment experienced by the ship moving at a constant velocity at an angle of attack in an ideal, non-viscous fluid. This will be explored in the next section.

2.3.2.4 Hull Lift Forces and Moments

Vehicle body lift in the horizontal plane results from the ship moving through the water at an angle of attack, causing flow separation and a subsequent pressure drop along the aft section of the hull. This pressure drop is modeled as a point pressure which is offset from the ship's body-fixed origin. This point force contributes a lift and moment about the origin. To estimate this effect, Hoerner's method is used ([7], [8]) which includes the Munk moment identified in the previous section.

Hull Lift Force

The hydrodynamic lift is based on the ship's angle of attack with respect to the flow, α_v.

$$\alpha_v = \tan^{-1}\left(\frac{-v}{u}\right) \approx \frac{-v}{u} \tag{2.25}$$

Therefore, the hull lift is defined as follows:

$$L_{hull} = -\frac{1}{2}\rho A_p C_L u^2 \tag{2.26}$$

A_p is the planform area (beam x length) and the lift coefficient is taken from [7], where C_L is the coefficient relationship for a planform aspect ratio of ~0.35:

$$C_L = \frac{\partial C_L}{\partial \alpha_v}\alpha_v = 0.146\left(\frac{-v}{u}\right) \tag{2.27}$$

Therefore, since the hull lift force is a force in the *Y*-direction, the hydrodynamic coefficient (dimensional) is defined as:

$$Y_{uv} = -\frac{1}{2}\rho A_p (0.146) \tag{2.28}$$

Hull Lift Moment

In a similar manner, the hull lift moment is generated, combining the Munk and lifting moments.

$$M_{hull} = -\frac{1}{2}\rho A_p L C_M u^2 \tag{2.29}$$

From Hoerner, the moment coefficient, CM, for a planform aspect ratio of 0.35 is given as:

$$C_M = \frac{\partial C_M}{\partial \alpha_v}\alpha_v = 0.035(1-\frac{T}{L})C_B\alpha_v = 0.0165\left(\frac{-v}{u}\right) \tag{2.30}$$

Therefore, the hull lift moment hydrodynamic coefficient (dimensional) is defined as:

$$N_{uv} = -\frac{1}{2}\rho A_p L(0.0165) \tag{2.31}$$

2.3.2.5 Bare Hull Hydrodynamic Coefficients from Planar Motion Mechanism

Planar Motion Mechanism data for the Wilderness Chesapeake Pro kayak was captured by Jeffrey Stettler at the US Naval Academy using a configuration depicted in Figure 2.4 [18]. The data from those tests measured the physical inertial properties of the model; however, there was a significant difference between the nonlinear added masses, moments of inertia, and centrifugal terms $\{ (X'_{\dot{u}} - m'),\ (Y'_{\dot{v}} - m'),\ (N'_{\dot{r}} - I'_{zz}),\ (X'_{vr} + m'),\ (Y'_r - m'U') \}$ of the model to the full-scale vessel. As such, the model inertial properties were subtracted from the data so the full-scale vessel inertial properties could be used instead in the equations of motion.

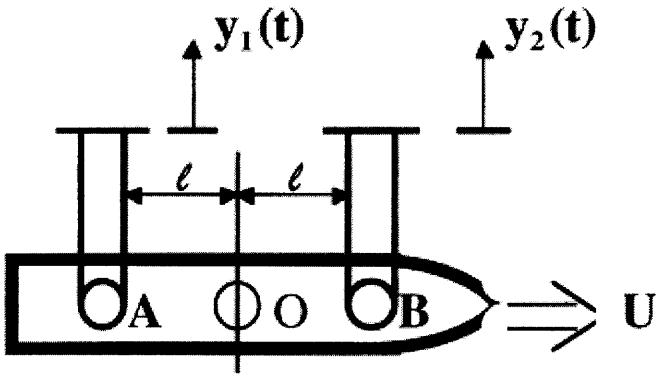

Figure 2.4: PMM measurement apparatus.

From the river tests of the kayak performed by Matthew Greytak [5], the hydrodynamic coefficients measured by Stettler were scaled to reflect the performance of the kayak in full-scale circumstances. The final non-dimensional hydrodynamic parameters with corrections applied are listed in Table 2.2.

Table 2.2: Final non-dimensional hydrodynamic coefficients taken from PMM measurement [18].

X-equation non-dimensional coefficient	Value ($x10^{-5}$)	Y-equation non-dimensional coefficient	Value ($x10^{-5}$)	N-equation non-dimensional coefficient	Value ($x10^{-5}$)
$(X'_{\dot{u}} - m')$	-680.9	$(Y'_{\dot{v}} - m')$	*-960.3*	$(N'_{\dot{r}} - I'_z)$	*-62.09*
X'_0	-67.2	Y'_0	3.331	N'_0	-6.895
X'_u	-148.1	Y'_{0u}	6.841	N'_{0u}	-18.95
X'_{uu}	-174.3	Y'_{0uu}	3.554	N'_{0uu}	-13.55
X'_{uuu}	-79.68	Y'_r	*-14.25*	$N'_{\dot{v}}$	*18.03*
$(X'_{ur} + m')$	74.54	$(Y'_r - m'u')$	*-392.6*	N'_v	*-315.7*
X'_{vv}	-273.4	Y'_{rr}	-149.8	N'_{vvv}	-3893
X'_{rr}	-105.8	Y'_v	*-120.3*	N'_r	*-221.1*
X'_{vvu}	-505.3	Y'_{vvv}	-39.94	N'_{rr}	-439.2
X'_{rru}	-80.67	Y'_{vur}	-3706	N'_{vur}	-1678
X'_{vru}	121.1	Y'_{vrr}	-4550	N'_{vrr}	-13796
		Y'_{vu}	-2156	N'_{vu}	-889.4
		Y'_{vuu}	-1336	N'_{vuu}	-695.2
		Y'_{ru}	-540.2	N'_{ru}	-615.0
		Y'_{ruu}	-134.3	N'_{ruu}	-556.7

2.3.3 Comparison of Hydrodynamic Coefficients

Applying the approximations derived above allows a comparison that can be made with the bare hull coefficients derived using the PMM on the model. This comparison is given in Table 2.3.

Table 2.3: Comparison of bare hull hydrodynamic coefficients.

Non-Dimensional Coefficient	Derived Value ($x10^{-5}$)	From Planar Motion Mechanism ($x10^{-5}$)	Comment
X_0	-67.30	-64.47	Resistance
$X_{\dot{u}}$	-65.97	-100.1	Added Mass
X_{uu}	-67.30	-57.56	Axial Drag
X_{vr}	-274.9	-506.3	Added Mass Cross-term
$Y_{\dot{v}}$	-274.9	-379.5	Added Mass
$Y_{\dot{r}}$	-42.58	-12.63	Added Mass
Y_v	-194.6	-100.4	Crossflow Drag
Y_r	+194.7	+188.3	Crossflow Drag
Y_{vu}	-1935	-1249	Hull Lift Force
Y_{ru}	-65.97	-673.6	Added Mass Cross-term
$N_{\dot{v}}$	-42.58	-9.148	Added Mass
$N_{\dot{r}}$	-22.26	-62.49	Added Mass
N_v	-247.8	-286.4	Crossflow Drag
N_r	-116.4	-90.47	Crossflow Drag
N_{vu}	-218.7	-567.1	Hull Lift Moment
N_{ru}	-42.58	-175.2	Added Mass Cross-term
N_{rvv}	-704.1	-874.6	Crossflow Drag

From this comparison it can be seen that many of the derived terms compare very favourably with those determined using PMM. As expected, the terms that compare the best are the linear terms; however, despite some of the derived non-linear terms being extremely different from the measured values, the impact to the expected maneuvering dynamics of the full-scale ship is small. This is demonstrated in Figure 2.5, where a turning circle using the derived terms is compared against the terms measured using PMM.

The differences that are noticed, however, may result from using the kayak as the physical model instead of a physical model that more closely resembles the DDG-1000, from which the derived hydrodynamic terms are calculated. The models notwithstanding, the differences in the non-linear terms do not contribute significantly to the overall predicted maneuvering performance of the vessel.

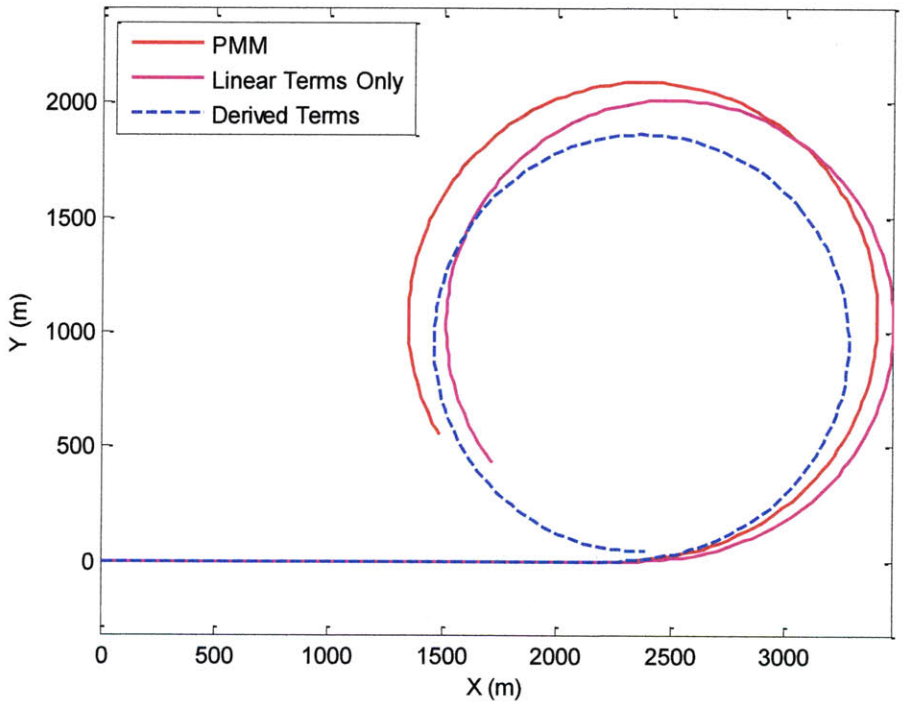

Figure 2.5: Comparison of the derived terms against the terms measured using PMM. It is notable that the derived terms yielded highly consistent results (rudder angled to 20 degrees).

2.3.4 Propulsive Forces and Moments

A ship moving forward through water has a force equal to the difference between the hull resistance and the propeller's thrust. From ([20], [21]) the non-linear open-water thrust provided by the propeller can be expressed as follows:

$$X_p = T_p = 2\rho n^2 D^4 \left[K_0 + K_1 J + K_2 J^2\right] \tag{2.32}$$

$$J = \frac{(1-w)u}{nD} \tag{2.33}$$

where n represents the propeller speed, D represents the propeller diameter, and J the advance coefficient. The constants (K_0, K_1, and K_2) represent the coefficients in a parabolic fit of the thrust coefficient to the open-water propeller curve (example shown in Figure 2.6). The term *(1 – w)* represents the Taylor wake fraction. Substituting for *J* gives a new expression for the propeller thrust:

$$T_p = \eta_1 n^2 + \eta_2 nu + \eta_3 u^2 \tag{2.34}$$

where:

$$\begin{aligned} \eta_1 &= 2\rho D^4 K_0 \\ \eta_2 &= 2(1-w)\rho D^3 K_1 \\ \eta_3 &= 2(1-w)^2 \rho D^2 K_3 \end{aligned} \tag{2.35}$$

In a similar manner, the propeller torque developed can be expressed as follows:

$$Q_p = \rho n^2 D^5 \left[Q_0 + Q_1 J + Q_2 J^2\right] \tag{2.36}$$

and substituting for *J* gives:

$$Q_p = \mu_1 n^2 + \mu_2 nu + \mu_3 u^2 \tag{2.37}$$

where:

$$\begin{aligned} \mu_1 &= \rho D^5 Q_0 \\ \mu_2 &= (1-w)\rho D^4 Q_1 \\ \mu_3 &= (1-w)^2 \rho D^3 Q_3 \end{aligned} \tag{2.38}$$

Representing propeller thrust and torque as a function of the propeller speed permits ship speed control by varying the propeller rotational speed. This becomes important as the overall ship performance model incorporates more detailed propulsion dynamics, necessitating a model of the driving engine.

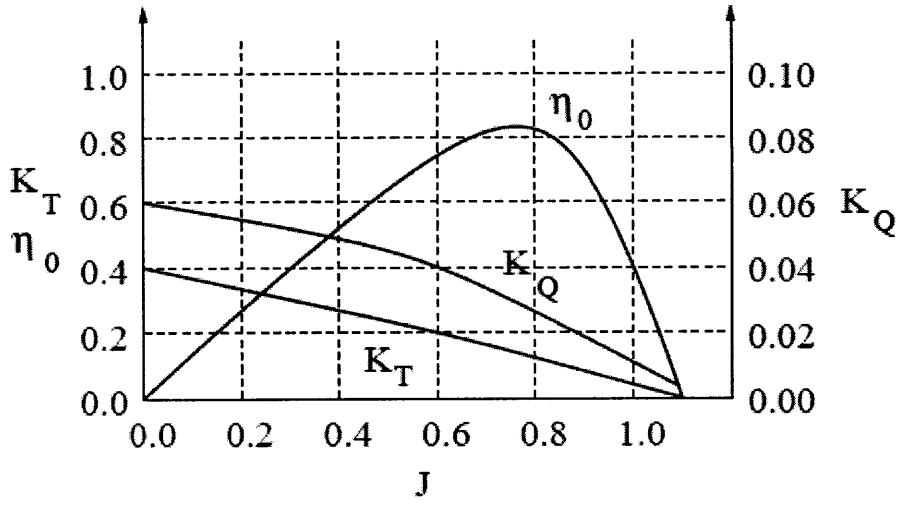

Figure 2.6: Typical open-water propeller curve showing K_T and K_Q curves which are used to formulate propeller thrust and torque.

2.3.5 Rudder Forces and Moments

The hydrodynamic coefficients previously discussed are for only the bare hull of the model without the effects of rudder interaction. Using foil theory, the rudders can be considered controllable foils with the provided mean chord and span. The coordinate system utilized for the analysis is provided in Figure 2.7. The rudder angle δ is taken positive towards the positive y-axis (causing a positive yaw motion), while r, v, and x_r are used with their algebraic value.

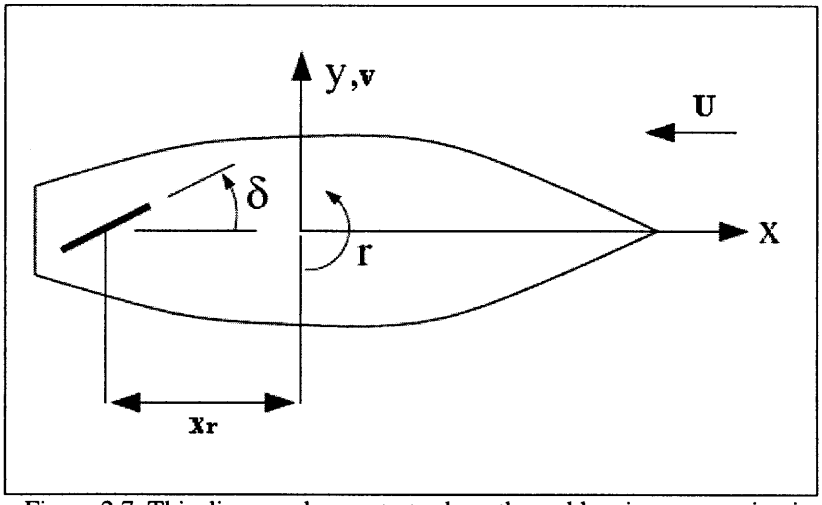

Figure 2.7: This diagram demonstrates how the rudder sign convention is applied.

Since the rudder moves with a side velocity $x_r r$ in addition to the sway component v, the angle of attack α between the rudder foil and the fluid velocity is given by the equation:

$$\alpha_R = \delta_R + \tan^{-1}\left(\frac{x_r r + v}{U}\right) \tag{2.39}$$

v and r are small compared to U. As a result, applying a small angle approximation:

$$\tan^{-1}\left(\frac{x_r r + v}{U}\right) \approx \frac{x_r r}{U} + \frac{v}{U} \tag{2.40}$$

Therefore, the resulting angle of attack, (neglecting turning effect for the time being):

$$\alpha_R = \delta_R + \frac{x_r r + v}{U} \tag{2.41}$$

This model may appear to be invalid at higher angles of attack (i.e. 20° rudder turn); however, the actual angle of attack is decreased rapidly as sway speed and yaw rate increase, changing the inflow velocity and angle. Changing inflow velocity will be explored in the next section.

Applying foil theory [21], the rudder acts as a lifting device when positioned at some angle of attack, α, measured with respect to the oncoming flow velocity, U. The lift force, *L*, acts perpendicular to the oncoming flow. Orthogonality of the lift and drag requires that the drag force, *D*, acts parallel to the flow as defined in Equations 2.42:

$$L = \frac{1}{2}\rho A_R U^2 C_L(\alpha)$$
$$D = \frac{1}{2}\rho A_R U^2 C_D(\alpha) \qquad (2.42)$$

where U is the fluid velocity as felt by the rudder (which can be approximated with the fluid velocity in-coming to the ship, neglecting additional turning effects for now), ρ is the water density, A_R is the total projected area of the rudder surface (A_R = chord*span) and $C_L(\alpha)$ and $C_D(\alpha)$ are the lift and drag coefficients as a function of α, respectively.

The drag of the rudder appendage is not insignificant and can account for up to 20% of the total ship resistance at the ship speeds that the model is being tested. The drag coefficient is taken directly using Peck's equation for control surfaces from [23]:

$$C_D(\alpha) = \frac{\partial C_D}{\partial \alpha}\alpha \approx \left[C_F \left(\frac{c}{c_f} + \frac{S}{A} + 40\left(\frac{t}{c_a}\right)^3 \right) \right] \alpha = 0.46\alpha \qquad (2.43)$$

where C_F is the skin friction line from ITTC 1957

c is the rudder chord length with t, c_a, and c_f sections of the control surface geometry (Figure 2.8)

S and A are the wetted surface area and frontal area at maximum thickness

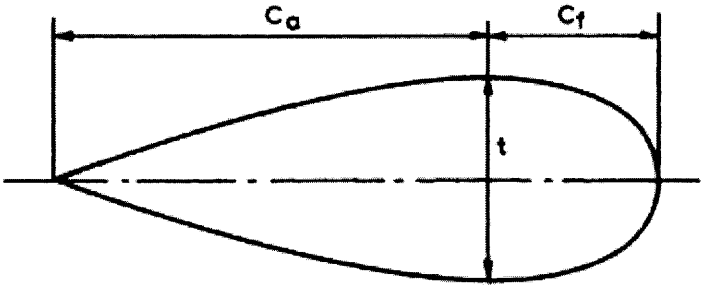

Figure 2.8: Definition of control surface section geometry for use in Peck's equation for the drag of control surfaces. [23]

Similarly, for small angles of attack α, the lift coefficient is nearly linear with α: i.e. $C_L = \frac{\partial C_L}{\partial \alpha}\alpha$, where $\frac{\partial C_L}{\partial \alpha}$ is the lift coefficient slope. For an aspect ratio > 1 the slope of the lift coefficient is given by the Hoerner's formula ([7], [8]):

$$\frac{\partial C_L}{\partial \alpha} = \frac{1}{\frac{1}{2\bar{a}\pi} + \frac{1}{\pi\ AR_{eff}} + \frac{1}{2\pi\ AR_{eff}^{\ 2}}} \qquad (2.44)$$

Since the rudder is attached to a reflective surface (ship), the effective span is twice its physical value, due to reflection, and thus the effective aspect ratio, AR_{eff}, as AR_{eff} = 2AR.

$$AR_{eff} = 2 \cdot AR = 2\frac{span}{chord} \approx 2.83 > 1 \qquad (2.45)$$

where α is in radians, $\bar{\alpha} \approx 0.90$. Substituting this into (2.44) gives $\frac{\partial C_L}{\partial a} \approx 3.24$.

Next, by substituting Equations (2.43) and (2.44) into (2.42), the following relation is obtained:

$$L = \frac{1}{2}\rho A_R U^2 \frac{\partial C_L}{\partial \alpha}\left(\delta_R + \frac{x_r r}{U} + \frac{v}{U}\right) \qquad (2.46)$$

Therefore, the lift force generates hydrodynamic terms that influence the previous bare-hull hydrodynamic coefficients Y_r, Y_v, N_r and N_v as shown in Equation 2.47.

$$Y_R = -L = -\frac{1}{2}\rho A_R U^2 \frac{\partial C_L}{\partial \alpha}\left(\delta_R + \frac{x_r r}{U} + \frac{v}{U}\right) = Y_\delta \delta_R + Y_{Rr} r + Y_{Rv} v \quad (2.47)$$

where

$$Y_\delta = -\frac{1}{2}\rho A_r U^2 \frac{\partial C_L}{\partial \alpha}$$

$$Y_{Rr} = \frac{Y_\delta x_r}{U}$$

$$Y_{Rv} = \frac{Y_\delta}{U}$$

and the hydrodynamic moment N on the rudder is:

$$N = Yx_r = N_\delta \delta + N_{Rr} r + N_{Rv} v \quad (2.48)$$

where

$$N_\delta = Y_\delta x_r$$

$$N_{Rr} = Y_{Rr} x_r$$

$$N_{Rv} = Y_{Rv} x_r$$

2.3.5.1 Accounting for turning motion and effective inflow velocity

As a vessel turns, its bow will angle inwards towards the center of the turning circle. This increases the sway and yaw rates of the stern and rudder. When this occurs, the inflow velocity can no longer be assumed to be attacking the rudder at the rudder angle only (Figures 2.9 and 2.10). Therefore, the instantaneous inflow velocity seen by the rudder as the vessel turns is expressed as:

$$U_{eff} = \sqrt{u^2 + (v + x_r r)^2} \quad (2.49)$$

and the instantaneous angle of attack becomes:

$$\alpha = \beta - \delta_R \quad (2.50)$$

where

$$\beta = \tan^{-1}\left(\frac{v + x_r r}{u}\right) \quad (2.51)$$

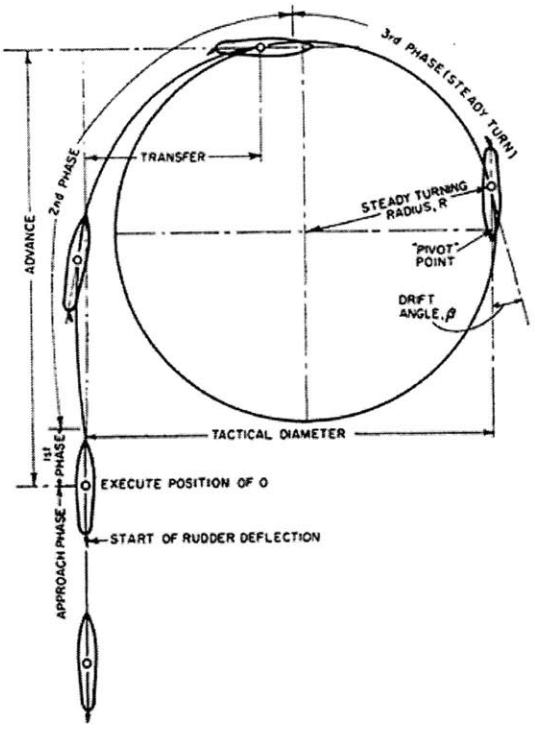

Figure 2.9: Turning circle of a ship with applied rudder angle (from [3]).

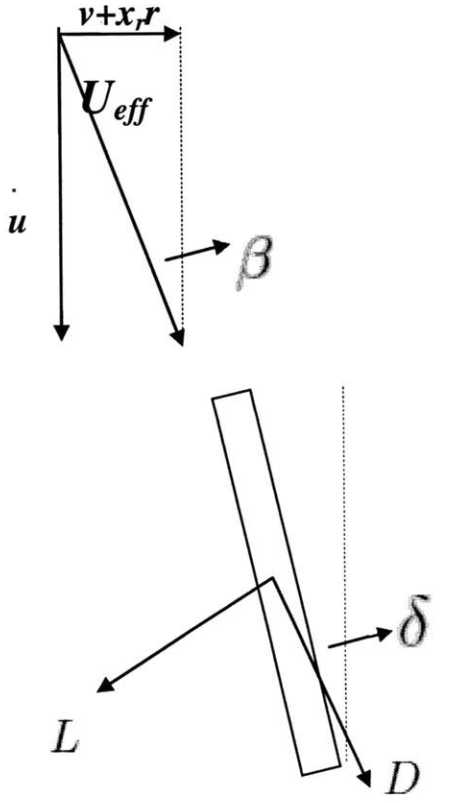

Figure 2.10: Effective inflow velocity and angle on rudder due to a turn.

Therefore, the forces and moments due to the rudder while maneuvering in the horizontal plane become:

$$\begin{aligned} F_x &= \text{sgn}(\alpha) L \sin(\alpha) - D\cos(\alpha) \\ F_y &= -\text{sgn}(\alpha) L \cos(\alpha) - D\sin(\alpha) \\ Q_z &= F_y x_r \end{aligned} \qquad (2.52)$$

In addition to the inflow velocity affecting the rudder, the effective inflow velocity will also impact the efficiency of the propellers. In general, as the inflow angle changes, the axial velocity will decrease, subsequently decreasing the advance coefficient, J. This tends to decrease the efficiency of the propeller in a turn.

2.4 A Model for Azimuthing Propulsion

Up to now, this thesis has looked at a model for the all-electric ship using conventional, or shafted, propulsion. There is also interest in predicting the maneuvering dynamics for a ship using azimuthing propellers. In general, the expaned non-linear hydrodynamic expression will remain the same from section 2.2 reiterated in Equation 2.53 below.

$$\begin{aligned} &m(\dot{u} - rv - r^2 x_G) = X_o + X_{\dot{u}}\dot{u} + X_u u + X_{uu}u^2 + X_{uuu}u^3 + X_{vv}v^2 + X_{rr}r^2 + X_{vvu}v^2 u + \\ &+ X_{rru}r^2 u + X_{vr}vr + X_{vru}vru + Ext.Forces \\ &m(\dot{v} + ru + \dot{r}x_G) = Y_{\dot{v}}\dot{v} + Y_{\dot{r}}\dot{r} + Y_v v + Y_{vvv}v^3 + Y_r r + Y_{rrr}r^3 + Y_{vrr}vr^2 + Y_{vu}vu + Y_{ru}ru \\ &+ Y_{vuu}vu^2 + Y_{rvv}rv^2 + Y_{ruu}ru^2 + Ext.Forces + ActuatorTerms \\ &I_{zz}\dot{r} + mx_G(\dot{v} + ru) = N_{\dot{v}}\dot{v} + N_{\dot{r}}\dot{r} + N_v v + N_{vvv}v^3 + N_r r + N_{rrr}r^3 + N_{vrr}vr^2 \\ &+ N_{vu}vu + N_{ru}ru + N_{vuu}vu^2 + N_{rvv}rv^2 + N_{ruu}ru^2 + ExtMoments + ActuatorTerms \end{aligned} \qquad (2.53)$$

The bare hull hydrodynamic coefficients can be assumed to remain the same, whether the PMM terms or the derived terms are used. The major difference now is how the external forces act on the bare hull and the actuator terms (i.e. rudder terms) from the previous model are removed. All maneuvering is done by placing the azimuth propellers at an

angle of attack relative to the flow. The coordinate reference frame for a ship using azimuth-podded propulsion is given in Figure 2.11.

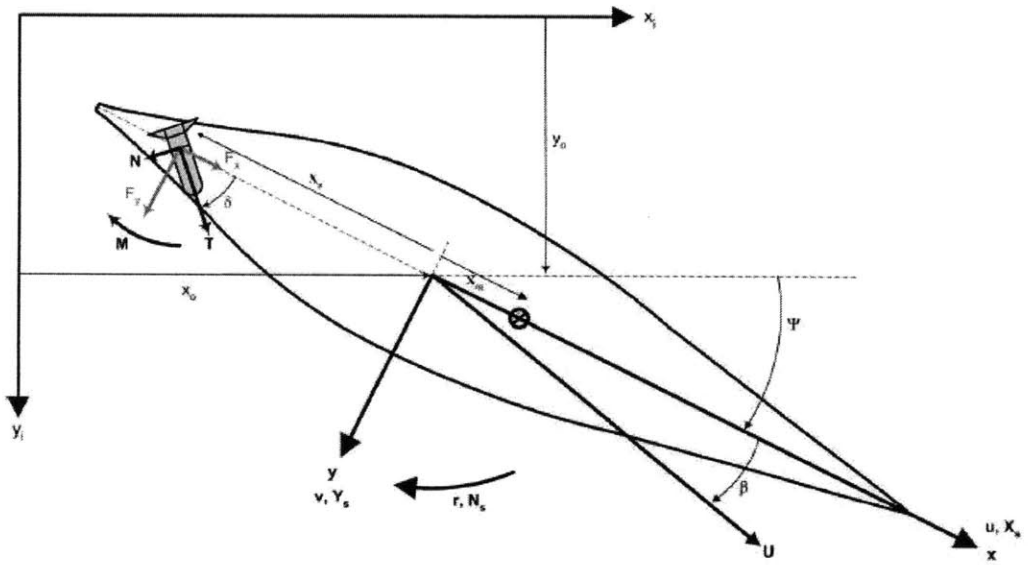

Figure 2.11: Coordinate reference frames for azimuthing propeller ship.

In 2004, Jeffrey Stettler developed non-dimensionalized force predictions for an azimuthing propeller and these are used in this thesis [18]. Figure 2.12 shows the non-dimensionalized forces for every possible azimuthing angle over a range of advance coefficients (from J=0 to 0.58). Applying these forces in place of the propeller and rudder of the previous model gives a prediction of a ship that is exceptionally more maneuverable than a conventionally propelled ship. This is to be expected as the azimuth propeller equipped ship can apply angles of attack up to 90 degrees. Figure 2.13 shows the turning circles for a ship equipped with azipods compared against conventionally shafted ships using the hydrodynamic coefficients derived in the earlier sections.

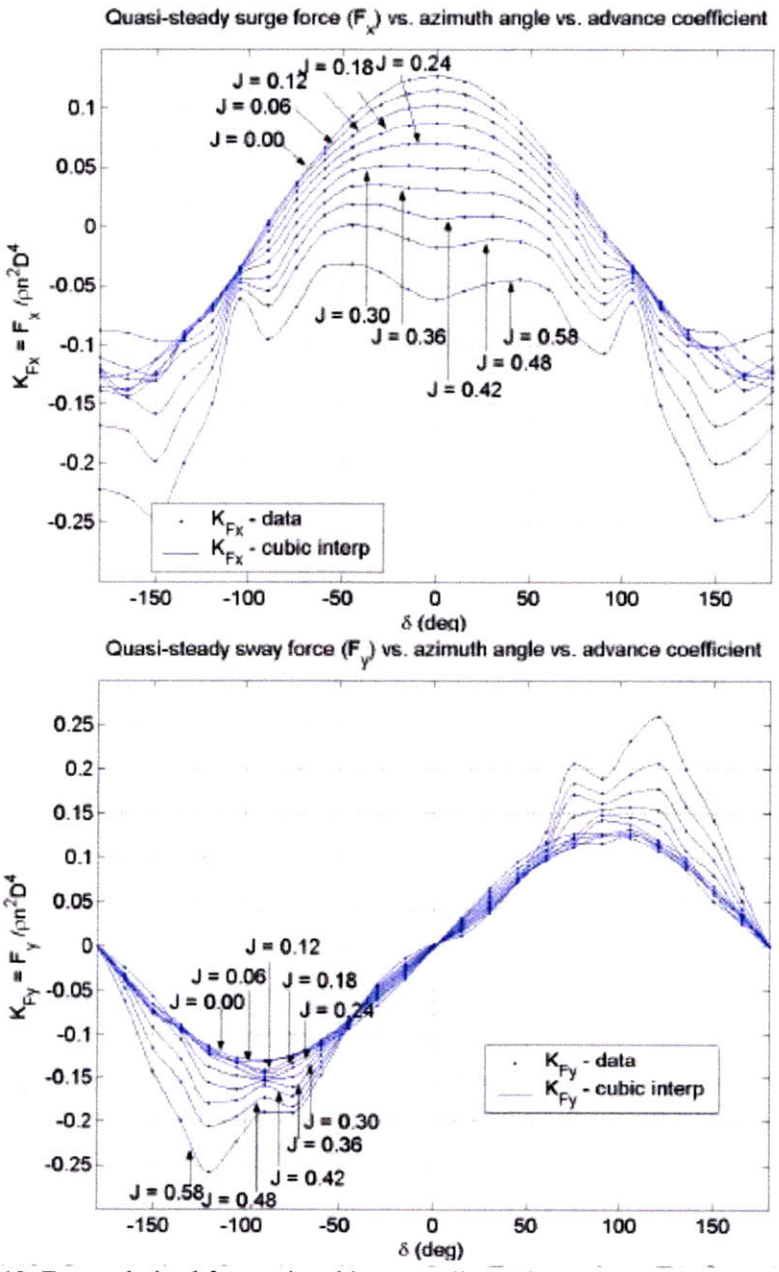

Figure 2.12: Forces derived from azimuthing propeller pods at all angles of attack.18].

A previous section compared the turning circles for the DDG-1000 using conventional (shafted) propulsion. Following the derivation of the azimuth podded forces presented here, it is equally important to compare how the ship will perform using azimuth podded propulsion angled to 90 degrees. Figure 2.13 shows this comparison. As expected, the turning circle is considerably tighter than when using conventional propulsion. It can be seen that the ship's forward motion (body-fixed) slows significantly as the transverse forces begin to dominate the propulsion.

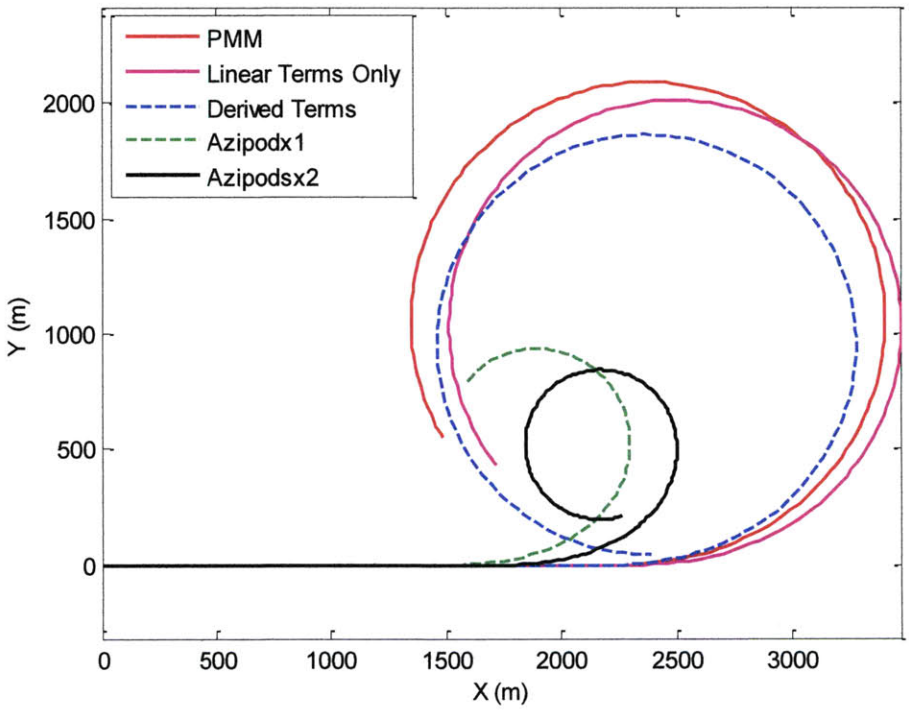

Figure 2.13: Turning circles for each set of hydrodynamic coefficients including azimuth podded propeller ship (both single and double pods). In this figure, the turning circle of the ship with azimuth podded propulsion is shown (Azipods angled to 90 degrees).

2.5 Chapter Summary

In this chapter, a model for the all-electric ship was presented based on the hydrodynamic coefficients for a kayak determined using PMM. Next, for this model, the non-linear governing equations of motion with the expanded hydrodynamic and external forces were presented. In order to determine the validity of this model, the bare-hull coefficients for the DDG-1000 were derived using various methods and applied to a conventionally powered ship and one that uses azimuth-podded propulsors (both single- and double-pods). Most importantly, by doing so, it has been shown that the Chesapeake Pro kayak is a valid model for the DDG-1000 about a 22 knot speed range.

This page intentionally blank

Chapter 3

Prediction of DDG-1000 Performance

The previous chapter demonstrated that the kayak can be used as a valid model for the DDG-1000 about a 22 knot speed range. This chapter presents simulation data that was performed using the MATLAB Simulink application. This gives an indication of the expected maneuvering performance of the all-electric ship in a calm sea and can be compared against known powering data from other applications to, again, assess the validity of the model. Specifically, the model is subjected to maneuvers in order to assess its stability. Furthermore, the simulated ship's propulsion system torque and thrust is measured in order to be compared against expected values in order to permit future optimization.

For this section, the simulation uses the hydrodynamic coefficients determined from the PMM measurements. These terms are used instead of the analytically derived terms because this model has more complete hydrodynamics and it has provided useful, consistent results over the speed range of interest.

The chapter sections are organized as follows:

3.1 Prediction of ship stability. The simulated model is subjected to zig-zag and spiral maneuvers in order to assess the ship's stability in the horizontal plane.

3.2 Prediction of ship propulsion performance. The simulated model performs turning circles with zero, fifteen, and twenty degrees rudder applied. The modeled system torques, powers,

3.1 Prediction of Ship Directional Stability

There are ship maneuvers that can be performed that will help determine the directional stability of a ship. Using the model's hydrodynamic coefficients, the model simulation can be given a rudder angle for a certain speed and the resulting maneuverability can be assessed. For this thesis, the model was subjected to simulations of the Dieudonne Spiral and the Zig-zag Maneuver.

3.1.1 Dieudonne Spiral

The Dieudonne spiral maneuver is the singularly definitive trial to determine a ship's directional stability characteristics. The maneuver is characterized by the following, described completely in [3]:

a) The ship begins on a straight-ahead course at a pre-determined speed and held on this course and speed for a pre-determined time. Once the speed and course is steadied, the propulsion plant is not modified for the full duration of the maneuver;

b) After the pre-determined time, the rudder is turned to a specific angle, δ_R, of about 20 deg to port, and held until the rate of change of yaw angle (r) maintains a constant value for a pre-determined time;

c) The rudder angle is next decreased by a five degrees, and held fixed again until the rate of change of yaw angle (r) maintains a constant value for a pre-determined time; and

d) The preceding procedure is repeated for rudder changes mving from 20 degrees port to 20 degrees starboard, back to 20 degrees port and finally back to midships.

Throughout the procedure, the steady yaw rates are recorded after the pre-determined time and plotted against the rudder angle, δ_R. This plot gives an indication of the stability

characteristics of the ship. Figure 3.1 shows an example plot of two ships with different directional stability characteristics.

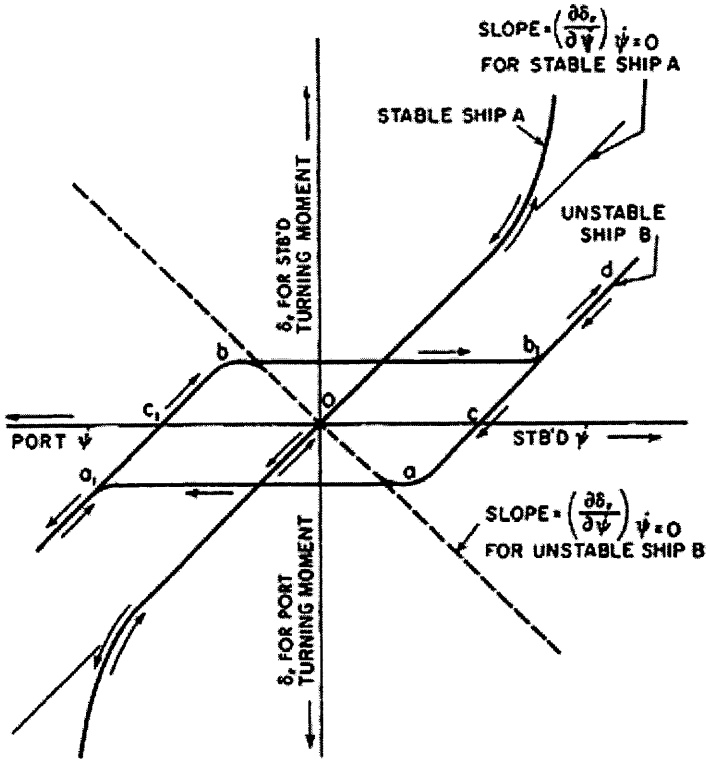

Figure 3.1: Example plot of Dieudonne spiral for directionally stable and unstable ships [from 3].

The plot shown in Figure 3.1 shows the distinction between two ships with different directional stability characteristics. Ship A possesses 'controls-fixed' straight line stability, which implies that the yaw-rate is constant for a given rudder angle, whether it's moving port or starboard. This is highly-desirable behaviour for small high-speed craft that require precision maneuvers. The 'hysteresis loop' created by ships with less directional stability, as for Ship B, may still be acceptable for large slower-moving ships with greater inertia. The plot for Ship B indicates a region where the ship may turn against its rudder; however, for slower and larger ships, the turning action is performed over a time-span of minutes, and corrective rudder can be applied quite easily.

Considering a ship's hydrodynamic characteristics derived using only linear theory, the slope of the yaw-rate curve can be predicted for a directionally stable ship using the following formula [3]:

$$\frac{r}{\delta_R} = -\left[\frac{Y_v' N_\delta' - N_v' Y_\delta'}{Y_v' N_r' - N_v'(Y_r' - \Delta)}\right] \tag{3.1}$$

where Δ is the ship's displacement.

For a directionally unstable ship, linear theory does not hold up and the hysteresis loop can not be predicted and must be plotted directly from measurement.

For the simulation of the DDG-1000, the directional stability results from a Dieudonne spiral maneuver is shown in Figure 3.2 for several pre-determined durations of two-minute, four-minute, and 'infinite'-duration. From this plot, it can be seen that there is indeed a hysteresis loop, predicting a directionally unstable ship. The two-minute duration implies that the ship is wildly unstable; however, it is important to allow sufficient time for conditions to 'steady' at each rudder angle. This is reflected in the plot of infinite duration where the it shows the characteristics of the hysteresis loop most clearly. In this case, the hysteresis loop is relatively small indicating that the ship is directionally unstable to only a small extent.

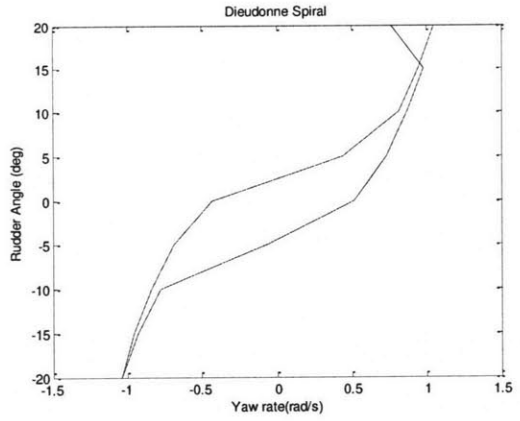

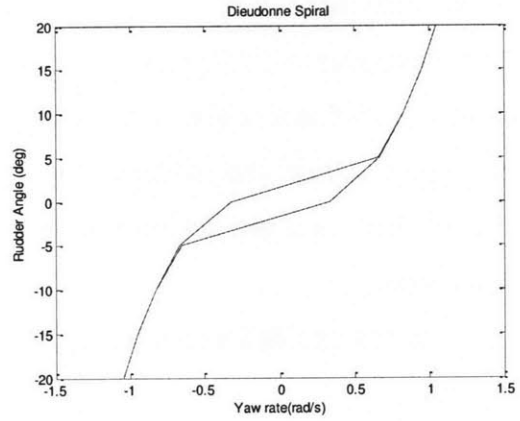

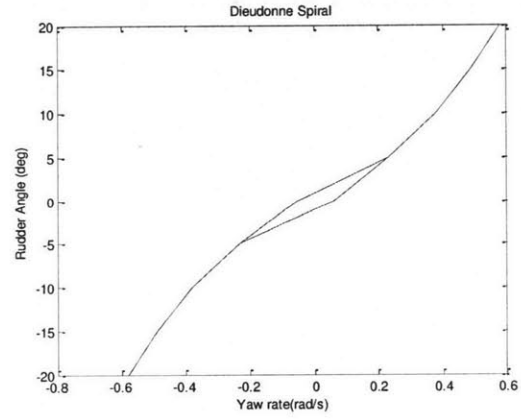

Figure 3.2: Plots of directional stability for several durations. Note how the hysteresis loop is more clearly visible and the ship demonstrates it's truer characteristics with greater duration.

3.1.2 Zig-zag Maneuver

Almost as important to the spiral maneuver in determining the directional stability of a ship is the zig-zag maneuver. The process of carrying out a zig-zag maneuver is described completely in [3] as follows:

a) The ship begins on a straight-ahead course at a pre-determined speed and held on this course and speed for a pre-determined time. Once the speed and course is steadied, the propulsion plant is not modified for the full duration of the maneuver;

b) Deflect the rudder to 20 degrees and hold until a pre-determined change of heading angle is reached (i.e. until a change in heading of 20 degrees);

c) At this point, deflect the rudder to the opposite angle of 20 degrees and hold until there is a pre-determined change in the heading angle on the opposite side.

d) This comprises one full execution cycle and can be repeated as often as necessary.

An example of the zig-zag test results is shown in Figure 3.3.

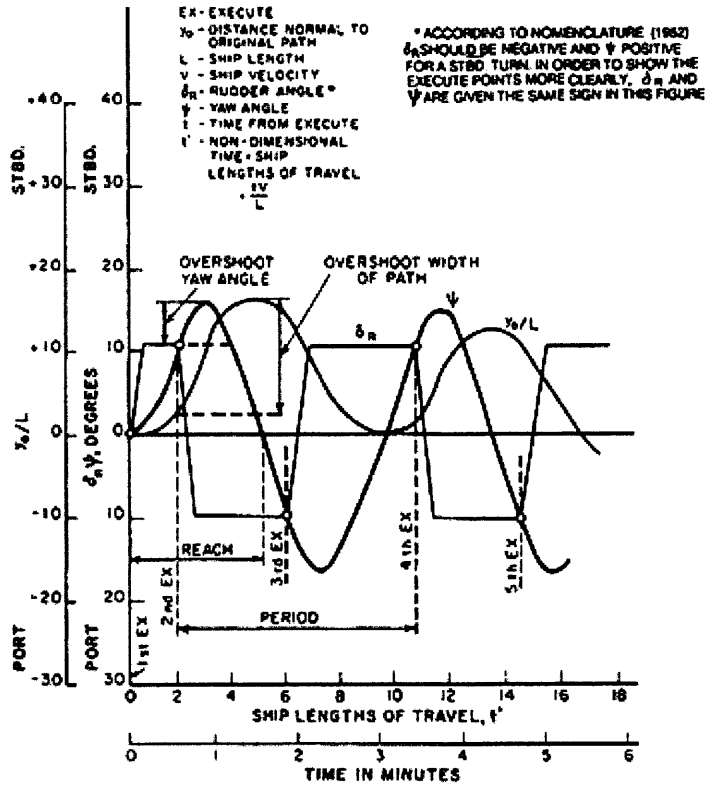

Figure 3.3: Example plot of zig-zag maneuver for a given ship over several executions [from 3].

This maneuver measures several parameters that describe the maneuverability of a ship. The first measurement is the 'reach', which is a direct measurement of a ship's ability to rapidly change direction. This measurement improves with rudder effectiveness and with decreased directional stability, as in the case of the simulated DDG-1000. Another two measurements are the 'overshoot yaw angle' and the 'overshoot width of path' which are numerical measures of counter-maneuvering ability and is indicative of the amount of anticipation required by a helmsman when performing maneuvers. Yaw-angle overshoot increases with decreased stability and with increased rudder effectiveness. Overshoot width of path decreases with both increased stability and increased rudder effectiveness [3].

The simulated DDG-1000 was subjected to a simulated zig-zag maneuver with the results presented in Figure 3.4. From this plot it can readily be seen that the yaw-angle overshoot is considerable. This is due in large part to the highly effective rudder and the ship's decreased directional stability. Making modification to the rudder could decrease

this to within tolerable levels, as would adding a heading controller to improve directional stability.

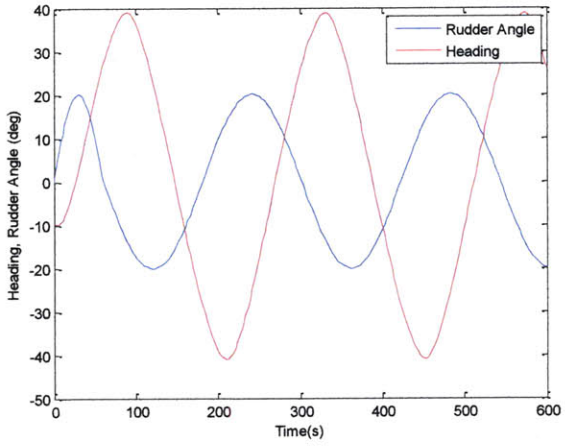

Figure 3.4: Zig-zag maneuver results for simulated DDG-1000.

3.2 Prediction of Ship Propulsion Performance

In addition to predicting the maneuvering performance of a ship, it is also of interest to know the powering requirements of the full-scale ship that can be derived from the model. By examining specific parameters, such as propeller speed and generated thrust, as the ship is made to meet a required speed and conduct turns at high speed, the simulated model can be validated against known, or expected, powering information about the DDG-1000.

Using the model's system configuration given previously (Figure 3.5), the interrelationships between the system parameters are easily recognized. The ship's main engines rotate at a set speed to generate the required electrical power through the power electronics. The electrical power induces torque in the induction motors that rotate the propeller shafts. The thrust and torque required by the propeller shafts is dependent on the hydrodynamic maneuvering coefficients considered previously.

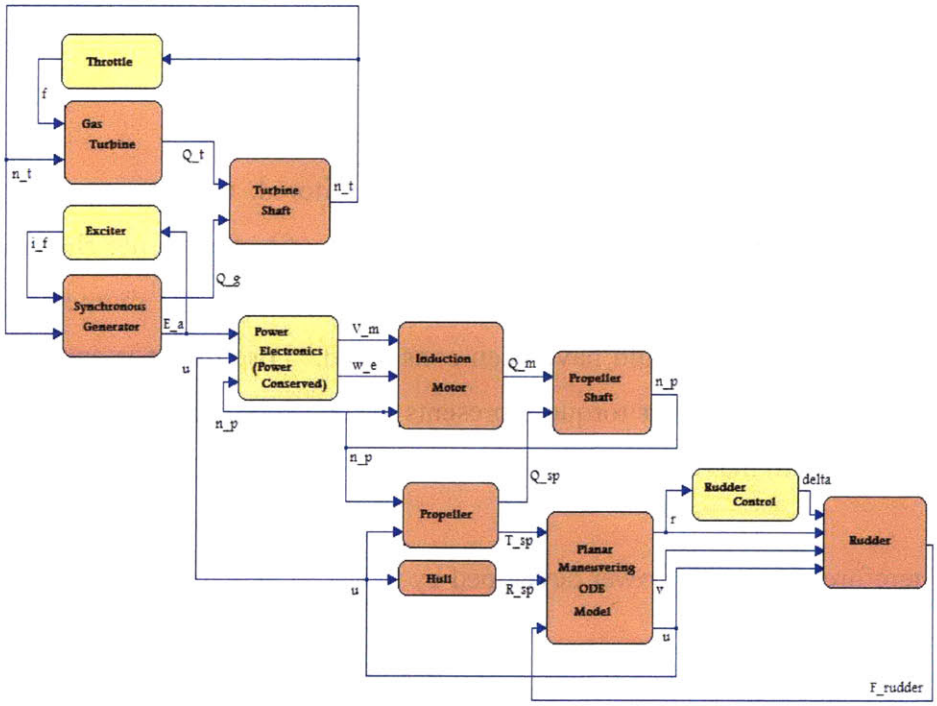

Figure 3.5: Simulated DDG-1000 model system configuration diagram

The model was developed by understanding the powering requirements that each system component in the model would be required to develop. Specifically, the relationships of interest are expressed in the following equations.

In order for the ship to move through the water, thrust forces are required to overcome ship's resistance, given by Equation 3.2.

$$T = k_T \rho n_{prop}^2 D^4 = R \cdot v_{ship}$$
$$Q_{prop} = k_Q \rho n_{prop}^2 D^5 \tag{3.2}$$

The thrust forcing and developed propeller torque is derived from the ship's propellers' open water diagram, which gives values for k_T and k_Q as functions of the ship's advance coefficient, given by Equation 3.3.

$$J = \frac{v_{ship}}{n_{prop} D} \tag{3.3}$$

Though the developed propeller torque is monitored, for the purposes of this thesis its effect is not being considered because of the use of two propeller shafts. Had there been an odd number of propeller shafts, the transverse forces and moments generated due to the uneven torques would have been considered. For now, it is enough to consider that the developed propeller torque represents system losses and it is desirable to minimize the torque and maximize the developed thrust.

Therefore, the usable power developed by the propellers is measured using Equation 3.4:

$$P_{thrust} = T \cdot v_{ship} \tag{3.4}$$

Next, having understood the ship powering requirements, the motor power required to make that happen is explored. Using the propeller shaft as the rotor, the expression for the induction motor power is given in Equation 3.5.

$$P_{motor} = 2\pi n_{prop} Q_{motor} \tag{3.5}$$

where Q_{motor} is the induced torque developed by the power electronics necessary to drive the shafts.

With the thrust power and the induction motor output power known, it is now possible to calculate the system's propulsive efficiency (Equation 3.6).

$$\eta_{prop} = \frac{P_{thrust}}{P_{motor}} \tag{3.6}$$

Graphical summaries of the simulations are presented in Figures 3.7 through 3.12 at the end of this chapter. These figures present data for the all-electric ship across varying pitch ratios, speed, and measurable parameters including propeller rpm, propeller efficiency, advance coefficient, induction motor output power and torque, and the power developed by the propeller thrust.

Using the relationships given above and from the data contained in the measured output, the simulation was run over a range of speeds (that still met the Froude similitude assumption) and compared against existing powering estimates for the DDG-1000 given in the USN's ship design software, ASSET (Advanced Surface Ship Evaluation Tool). The resultant comparison is given in Table 3.1 for zero rudder and a propeller pitch ratio of $P/D = 1.4$.

Table 3.1: Validation of simulated model output motor power. (Zero rudder, P/D=1.4)

Speed (knots)	ASSET (MW)	Simulation (MW)
20	9	12.1
22	12.5	15.9
24	17.1	20.4
26	22.8	25.7
28	30.4	31.9
30.2	43.6	40.1

It can be seen that the simulation provides very consistent results with expected values, validating the Simulink model for the given speed range. Of note, however, is that ASSET achieves the max powering (30.2 knots) using a propeller of 5.5m rotating at 150 rpm, while the Simulink model required the same propeller to rotate at 206 rpm. In the latter case, this is within the region of expected and typical shaft rotational speeds for a warship of this class.

Further validation of the Simulink model is evident when the output motor torque values are compared against the expected endurance, maximum and maximum sustained speeds (20, 30, and 28.4 knots, respectively) derived using ASSET in Table 3.2. Again, the values shown in the table are for zero rudder and a propeller pitch ratio of $P/D = 1.4$.

Table 3.2: Validation of simulated model induction motor torques. (Zero rudder, P/D=1.4)

Speed (knots)	ASSET (kN-m)	Simulation (kN-m)
20	618	605
28.4	1515	1659
30	1800	1772

From the output motor torque values the Simulink model is further validated. The simulated model compares very well with the expected torque values at the given speeds. For further validation, the simulated output motor torque values were captured for the vessel making high speed turns, as in Figure 3.6. As expected, for turns applying greater than 25 degree rudder, the output motor torque values increased by approximately 20%, which is consistent with expected output torque increases for ships of this class.

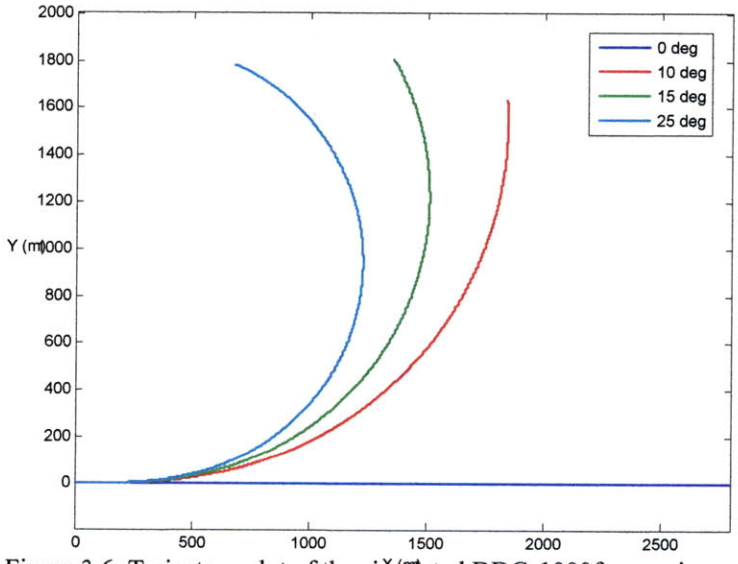

Figure 3.6: Trajectory plot of the simulated DDG-1000for varying rudder angles

3.3 Chapter Summary

This chapter has shown that the Simulink model developed for the DDG-1000 demonstrates directional stability characteristics consistent with a ship of this size and class. Furthermore, the model demonstrates propulsion performance characteristics highly consistent with the expected performance of the DDG-1000 and is a useful basis for further simulation. From this baseline model, it is possible to begin optimizing several facets of the system to improve overall predicted performance. Appendix II gives a cavitation analysis for the propeller that is currently fitted in the DDG-1000 as a means to predict expected performance and propose changes, as necessary.

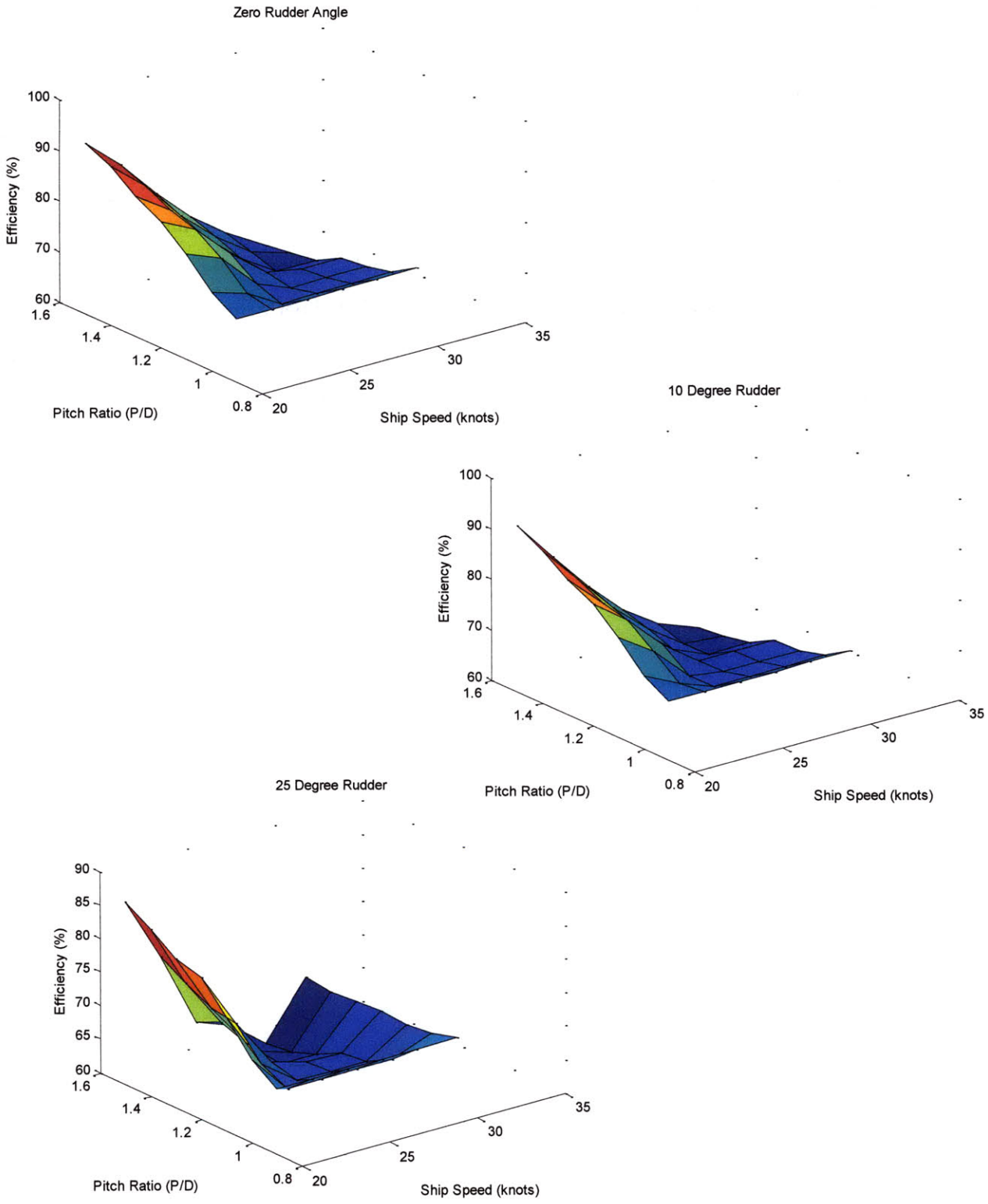

Figure 3.7: Plots of propulsion efficiency for conventional propulsion over a range of speeds and rudder turning angles.

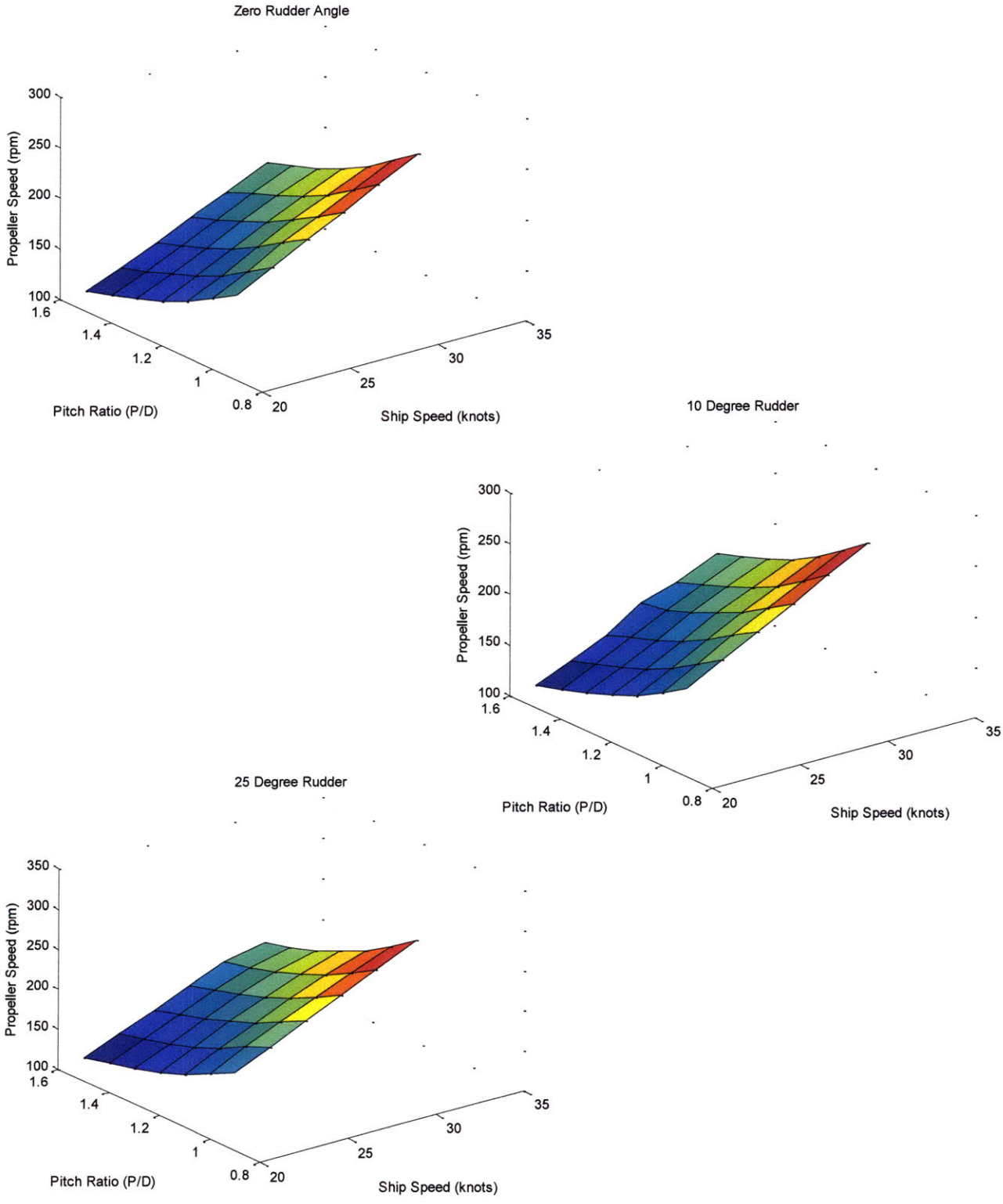

Figure 3.8: Plots of propeller speed for conventional propulsion over range of speeds and rudder turning angles.

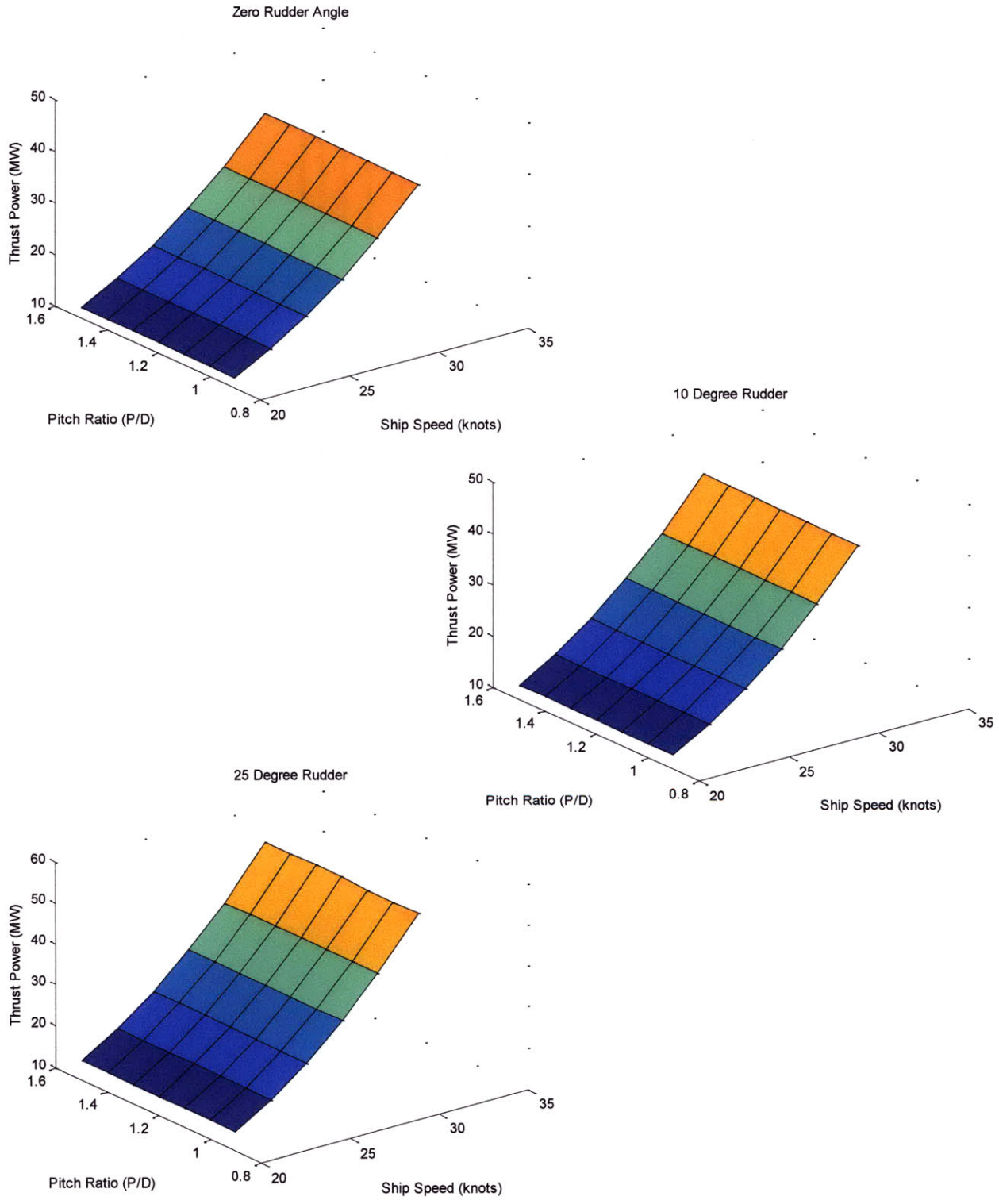

Figure 3.9: Plots of propeller thrust power for conventional propulsion over range of speeds and rudder turning angles.

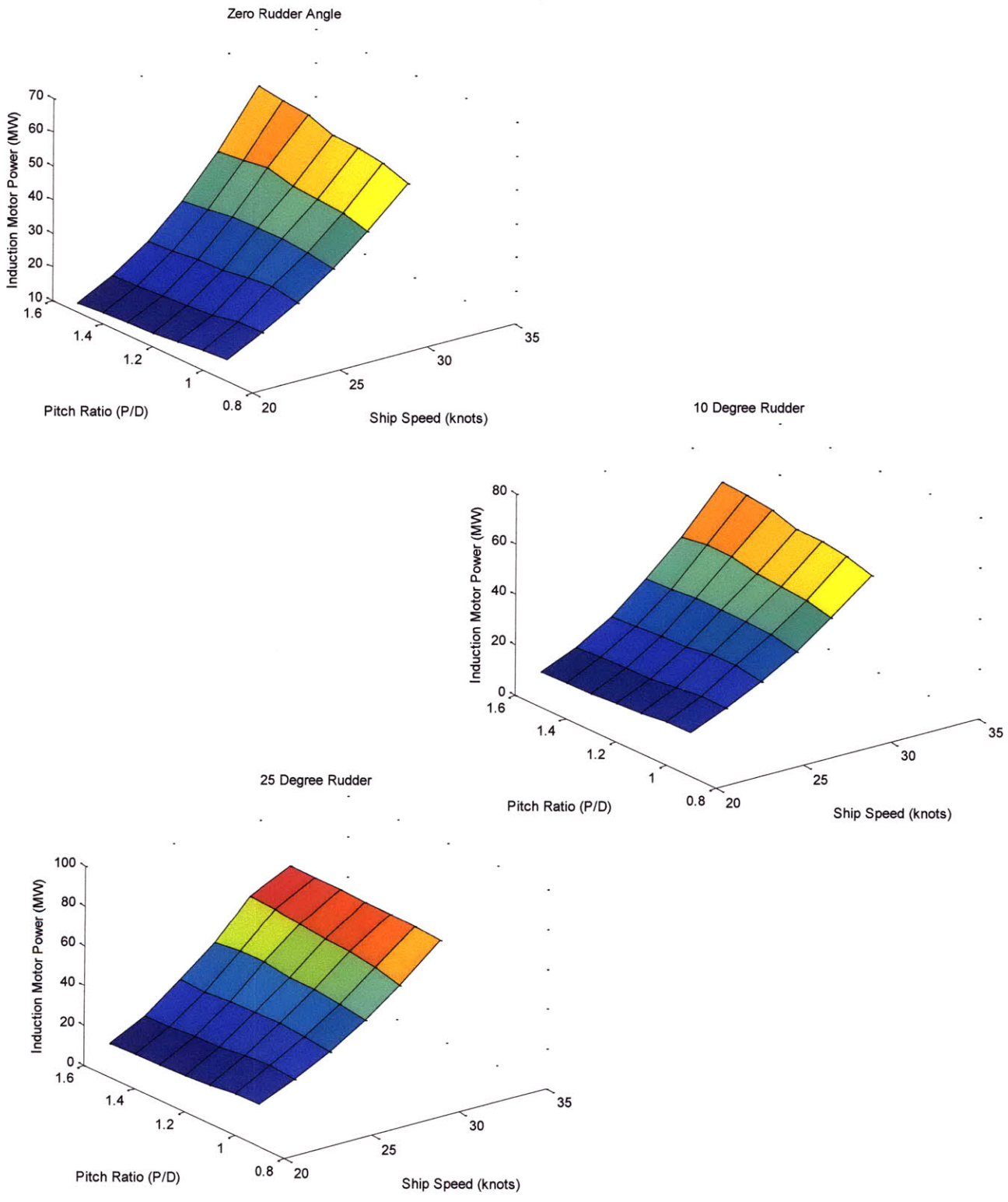

Figure 3.10: Plots of induction motor power for conventional propulsion over range of speeds and rudder turning angles.

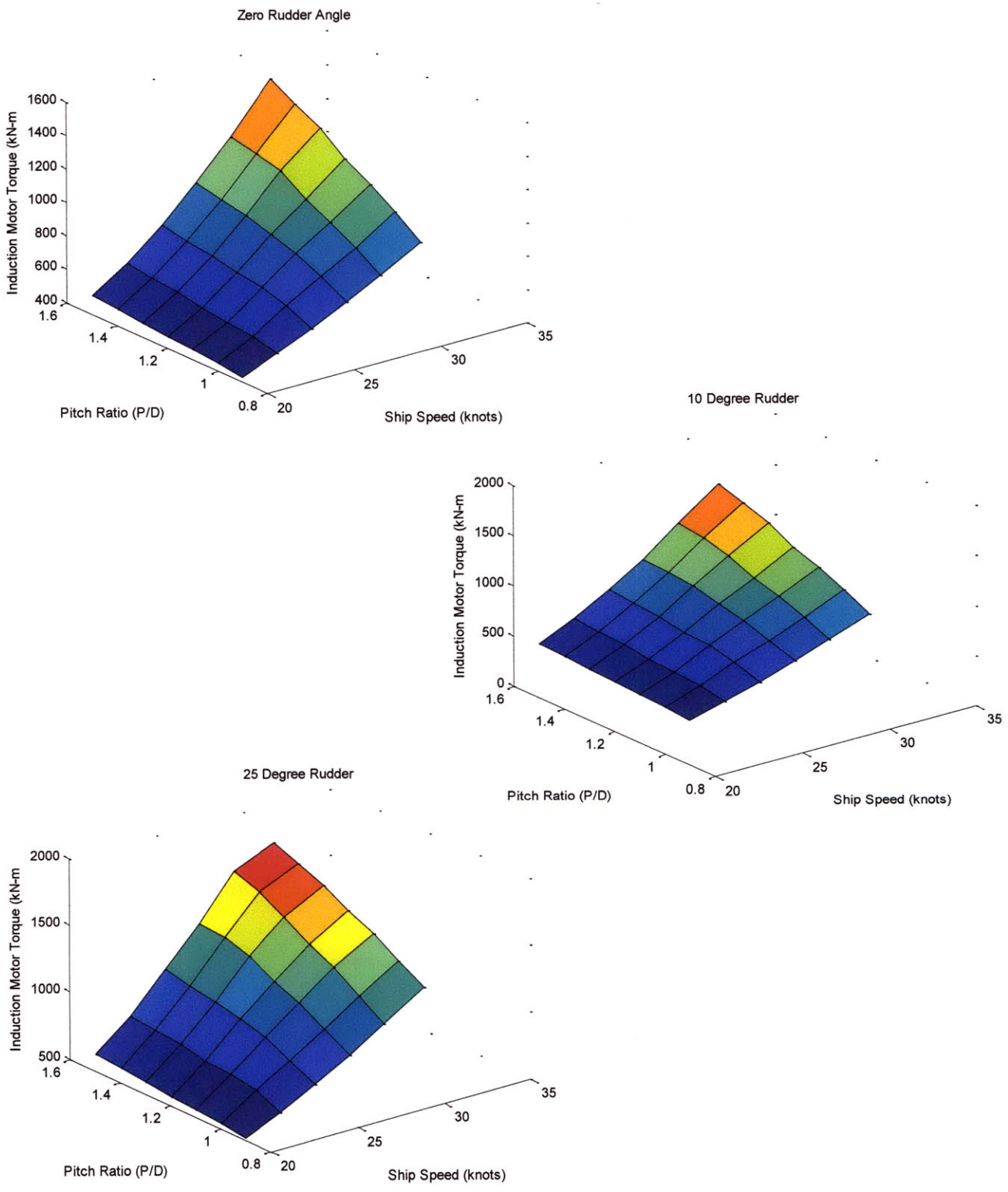

Figure 3.11: Plots of induction motor output torque for conventional propulsion over range of speeds and rudder turning angles.

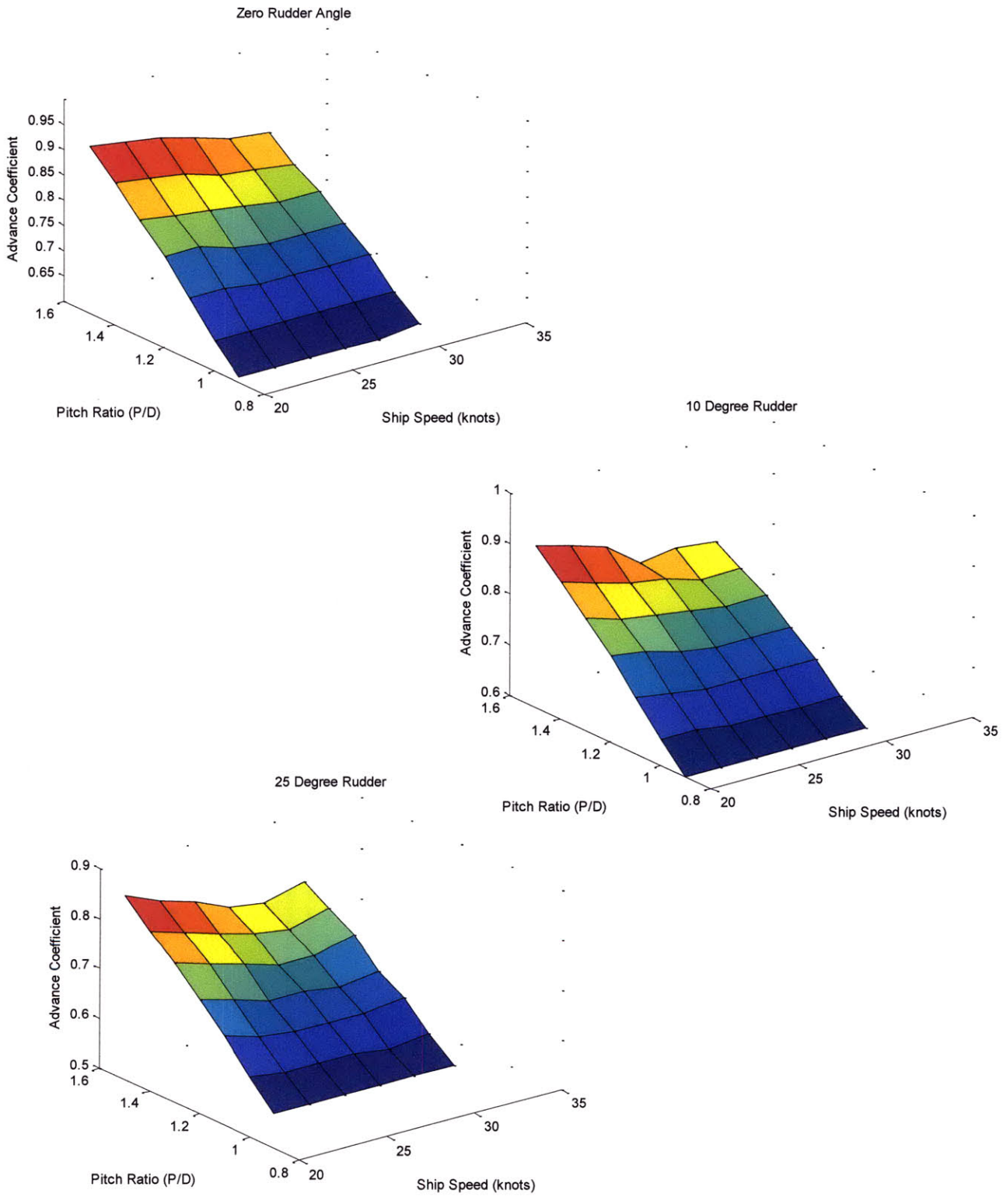

Figure 3.12: Plots of advance coefficients for conventional propulsion over range of speeds and rudder turning angles.

This page intentionally blank

Chapter 4

Conclusions and Future Work

A dynamic model of the DDG-1000 was initially created with the intent of being able to predict the performance of the vessel at sea in the absence of a physical model of the platform. To achieve this, the non-linear hydrodynamic equations were derived by applying a Taylor series expansion that would provide coefficients up to the third order. Exploiting symmetry as much as possible, the equations and terms were simplified significantly. Then, the hydrodynamic coefficients were derived using analytical methods to give a fully derived hydrodynamic model of the DDG-1000. This model was compared against the Chesapeake Pro kayak, whose hydrodynamic terms were derived using planar motion mechanism, and found to be very comparable. Thus, the Chesapeake Pro kayak's hydrodynamic coefficients were deemed acceptable for use to simulate and predict the performance of the full-scale Naval vessel.

Several simulations using MATLAB Simulink were conducted over a speed range defined by the Froude similitude between the kayak and the DDG-1000. These simulations predicted highly consistent results in keeping with the expected performance of a ship of this size and class. The performance forms the basis for potential optimization of the overall system, from the main engines generating electrical power through the power electronics to the induction motor providing the output torque to drive the propellers and the ship.

Potential future development of this model is, as mentioned, optimization of the propulsion systems and their respective controllers. For example, the main engine controller can be optimized using a Kalman filter residue reduction method. Also, the propellers can be optimized to reduce likelihood of cavitation inception. The non-linear maneuvering dynamics can be applied to develop a proper heading control system for the ship.

Most importantly, the current model only looks at the maneuvering and propulsion performance in a calm sea, but a better picture of performance can be realized if the linear and non-linear wave forces were added to the simulation forces acting on the vessel in additional degrees of freedom, most notably heave and pitch. Therefore, as the vessel maneuvers in a random sea, the added mass and damping forces for heave and pitch can be determined and applied to the overall forces acting on the system. It is understood that this development is currently being attempted.

Previous work of this type has often focused on the prediction of hydrodynamic coefficients through the use of system identification, a process most thoroughly initiated by Hwang et al. [9]. The method involves using the maneuvering data of the full-scale ship to estimate the coefficients that were derived from model-testing. Conversely, in the absence of model-testing, this thesis predicted the hydrodynamic coefficients using analytical methods and used these to estimate the maneuvering and propulsive performance. Future work may include the use of system identification from maneuvering data of the full-size DDG-1000 to further validate the results obtained here.

Bibliography

1. Abkowitz, M.A., *Stability and Motion Control of Ocean Vehicles*, The M.I.T. Press, Cambridge, MA, 1969.

2. Blevins, R.D., *Formulas for Natural Frequency and Mode Shape*. Robert E. kreiger Publishing Co. Malabar, FL, 1984.

3. Crane, C.L., Eda, H., and Landsburg, A., *Principles of Naval Architecture*, Chapter IX (Controllability), Lewis, E.V. (Ed.), The Society of Naval Architects and Marine Engineers, Jersey City, New Jersey, 1988.

4. Fossen, T.I., *Guidance and Control of Ocean Vehicles*. John Wiley & Sons, New York, 1994.

5. Greytak, M.B., *High Performance Path Following for Marine Vehicles Using Azimuth-Podded Propulsion*. MSc Thesis, Massachusetts Institute of Technology, 2006.

6. Hayes, M.N., *Parametric Identification of Nonlinear Stochastic Systems Applied to Ocean Vehicle Dynamics*. PhD Thesis, Massachusetts Institute of Technology, 1971.

7. Hoerner, S., *Fluid Dynamic Lift*. Hoerner Fluid Dynamics, Vancouver, WA, 1985.

8. Hoerner, S., *Fluid Dynamic Drag*. Hoerner Fluid Dynamics, Vancouver, WA, 1992.

9. Hwang W., *Application of System Identification to Ship Maneuvering*. PhD Thesis, Massachusetts Institute of Technology, 1980.

10. Inoue, S., Hirano, M., and Kijima, K., "Hydrodynamic Derivatives on Ship Manoeuvring," *International Shipbuilding Progress*, vol. 28, pp. 112–125, 1981.

11. Islam, M.F., Veitch, B., Liu, P., "Experimental Research on Marine Podded Propulsors," *Journal of Naval Architecture and Marine Engineering*, vol. 4, pp. 57-71, December 2007.

12. Kerwin, J.E., Hydrofoils and Propellers, Course notes for MIT course 2.23, Hydrofoils and Propellers, Department of Mechanical Engineering, Massachusetts Institute of Technology, Cambridge, MA, 2001.

13. Kim, J., Kim, K., Hang, C., et al., "Estimation of Hydrodynamic Coefficients for an AUV Using Nonlinear Observers," *IEEE Journal of Oceanic Engineering*, vol. 27, pp. 830-840, October 2002.

14. McTaggart K.A., Simulation of Hydrodynamic Forces and Motions for a Freely Maneuvering Ship in a Seaway. (DRDC Atlantic TM 2005-071). Defence Research and Development Canada – Atlantic, 2005.

15. Ojeda, Q., *Robust Control Design and Simulation of the Maneuvering Dynamics of an Arleigh Burke Class Destroyer.* MSc Thesis, Massachusetts Institute of Technology, 1999.

16. Rajesh, G., and Bhattacharyya, S.K., "System Identification for nonlinear maneuvering of large tankers using artificial neural network," *Applied Ocean Research,* vol. 30, pp. 256-263, October 2008.

17. Rentschler, M.E., *Dynamic Simulation Modeling and Control of the Odyssey III Autonomous Underwater Vehicle.* MSc Thesis, Massachusetts Institute of Technology, 2003.

18. Stettler, J.W., *Steady and Unsteady Dynamics of an Azimuthing Podded Propulsor Related to Vehicle Maneuvering.* PhD Thesis, Massachusetts Institute of Technology, 2004.

19. Szeto F.F., *System Identification from Ship Maneuvers in Currents*, MSc Thesis, Massachusetts Institute of Technology, 1977.

20. Taylor, M.E., *System Identification of an Arleigh Burke Class Destroyer Using an Extended Kalman Filter.* MSc Thesis, Massachusetts Institute of Technology, 2000.

21. Triantafyllou, M.S., Hover, F.S., and Stettler, J.W., "Preliminary results of testing on the dynamics of an azimuthing podded propulsor relating to vehicle maneuvering," *First International Conference on Technological Advances in Podded Propulsion,* Newcastle-upon-Tyne, UK, pp. 321-337, April 2004.

22. Triantafyllou, M.S., and Hover, F.S., *Maneuvering and Control of Marine Vehicles*, Course notes for MIT course 2.154, Maneuvering and Control of Marine Vehicles, Department of Mechanical Engineering, Massachusetts Institute of Technology, Cambridge, Massachusetts, 2001.

23. Van Manan, J.D., and Van Oossanen, P., *Principles of Naval Architecture*, Chapter VI (Propulsion), Lewis, E.V. (Ed.), The Society of Naval Architects and Marine Engineers, Jersey City, New Jersey, 1988.

24. Viviani, M. et al., "Identification of hydrodynamic coefficients from standard maneuvers for a series of twin-screw ships," pp. 99-108, 2003

25. Woud, H.K., and Stapersma, D., *Design of Propulsion and Electric Power Generation Systems.* Institute of Marine Engineering, Science, and Technology, London, 2003.

26. Yee, K.Y., and Rhee, K.P., "Identification of hydrodynamic coefficients in ship maneuvering equations of motion by Estimation-Before-Modeling technique," *Journal of Ocean Engineering*, vol. 30, pp. 2379-2404, 2003.

27. Zill, D.G., and Cullen, M.R., *Differential Equations with Boundary Value Problems*, Ostedt, G. (Ed.), Brooks/Cole Publishing Co., Pacific Grove, CA, 1997.

This page intentionally blank

Appendix I

Description of the Physical Model

The physical model used to approximate the DDG-1000 is derived from the bare hull nonlinear hydrodynamic coefficients measured using the Planar Motion Mechanism on a 3.72 meter Wilderness Chesapeake Pro kayak with a 0.7 meter beam and weighing 122.5 kg, depicted in Figure I.1 ([5],[18]).

Figure I.1: Depiction of autonomous kayak used to approximate the DDG-1000

The physical dimensions of the kayak and the DDG-1000 are given in Tables I.1 and I.2, respectively.

Table I.1: Physical properties of the Chesapeake Pro kayak.

Length	3.66	m
Weight	142.16	kg
Izz	1.53	kg*m^2
Test speed	1.60	m/sec
Water density	1000	kg/m^3

Table I.2: Physical properties of the full-scale all-electric DDG-1000.

Length	182.84	m
Beam	24.08	m
Displacement	1.325E+07	kg
Izz	8.023E+08	$kg*m^2$
Wetted surface area	4634	m^2
Design speed	11.32	m/sec
Rudder chord	3.658	m
Rudder span	5.182	m
Location of rudders	73.136	m aft of CG
Location of ship's CG	2.7432	m aft of midships
Water density (salt water)	1025	kg/m^3
Propeller Diameter	5.5	m

Appendix II

Cavitation Analysis

It was of interest to determine the likelihood of cavitation inception for the propeller that is currently considered for the DDG-1000 over a range of rotational speeds. The physical details of this propeller are detailed in Table II.1.

Table II.1: Physical data of the DDG-1000 propeller

Diameter	5.5	m
Number of blades	5	
Pitch ratio	1.4	
Rotational speed	100 to 250	rpm
Ship speed	11.5	m/s
Thrust	1100	kN (at 22 knots)
Depth of propeller hub	8	m
Blade area ratio for Wageningen 5.55	0.680	
Vapour pressure of water	1700	Pa

In order to determine if the propeller will cavitate, Burrill's method provides a useful tool to evaluate the extent of cavitation at the beginning of the design stage. Burrill's method uses a series of parametric curves to gauge the likelihood and extent of cavitation in a region. This method is satisfactory for the purposes of this analysis; however, for a more detailed design or optimization, additional tools to determine the pressure and vortex distribution at each point in the blade could be developed. This would give a better understanding of the actual distribution of the cavitation.

Burrill's Method

The cavitation inception is calculated by choosing a point on the blade at 0.7R

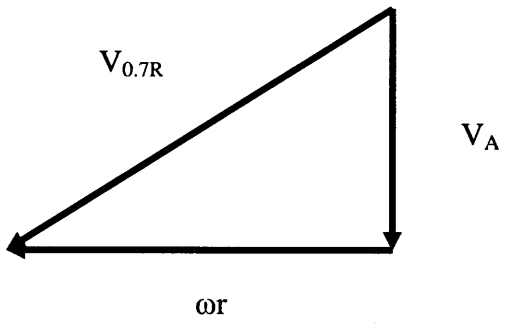

Figure II.1: Vector diagram of rotating propeller blade at a radius of 0.7R

From Figure II.1, it can be seen that the velocity seen by the blade at that point is:

$$V_{0.7R}^2 = (V_A^2 + (0.7n\pi D)^2 \tag{II.1}$$

where n is the propeller rotational speed.

Next, using the given blade-area ratio (BAR; the ratio of the effective area to the actuator disk area), the projected blade area, A_P, can be calculated

$$BAR = \frac{A_E}{A_O} = 0.680$$

$$\therefore A_E = \frac{\pi D^2}{4}(0.680) = 16.16m^2$$

$$A_E \approx A_D \tag{II.2}$$

From Taylor's relationship, the projected area can be calculated:

$$A_D = \frac{A_P}{(1.067 - 0.229)\frac{P}{D}} \tag{II.3}$$

Therefore,

$$A_P = 12.062m^2$$

Then, using Burrill's criteria to calculate the thrust coefficient and the cavitation number (Equations II.4 and II.5), the parameters necessary to determine the extent of cavitation can be plotted over the propeller rotational speed range, n.

Calculate thrust coefficient:

$$\tau_c = \frac{T}{0.5\rho A_P V_{0.7R}^2} \tag{II.4}$$

Calculate cavitation number:

$$\sigma_R = \frac{(P_O - P_V)}{0.5\rho V_{0.7R}^2} \tag{II.5}$$

The results are plotted on Burrill's cavitation criteria curves in Figure II.2

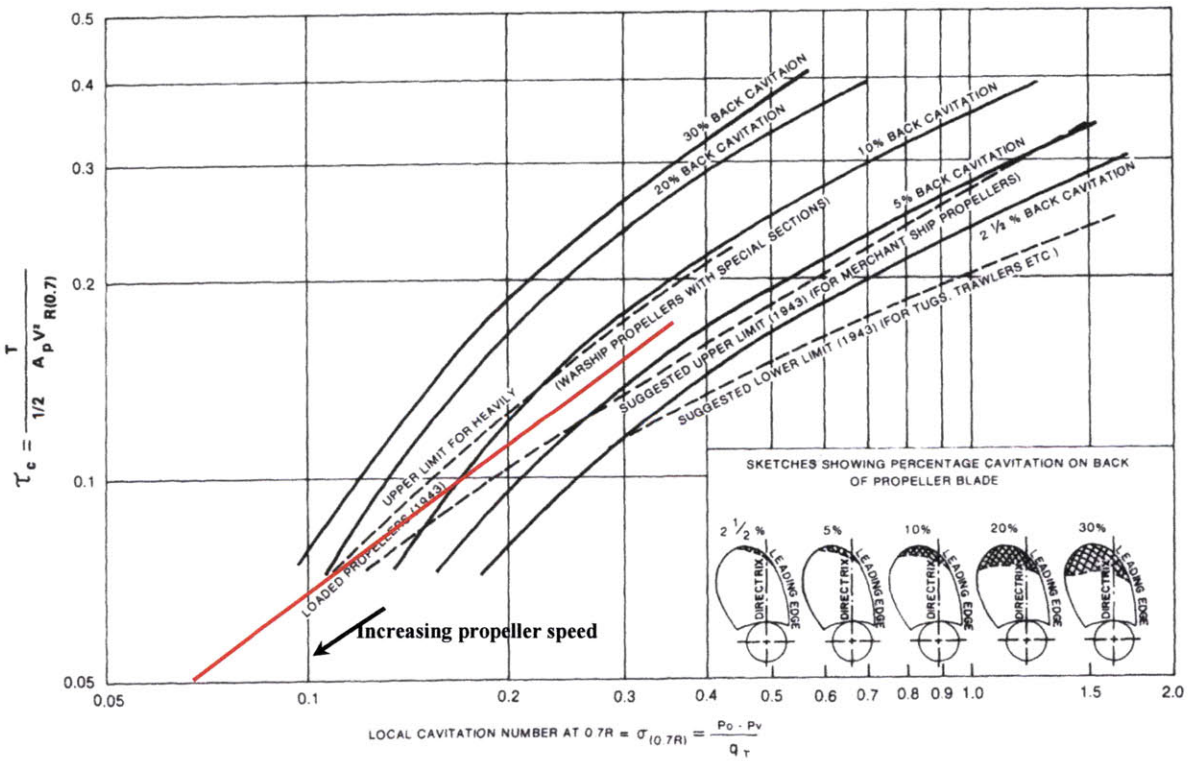

Figure II.2: Burrill's cavitation criteria showing the plot of the DDG-1000 propeller and indicating the extent of cavitation, in red. [from [23]]

From Figure II.2, it can be seen that the DDG-1000, using two propellers, stays within the upper limit for heavily loaded propellers, which is recommend for naval warships; however, at the higher speed ranges, the inception of cavitation is exceeding 20%. Furthermore, as the ship speed increases, the heavier loaded propeller will begin to see much more cavitation.